

**A SPATIAL ENHANCEMENT SCHEME WITH  
SUPERVISED PIXEL CLASSIFICATION FOR  
BLOOD VESSEL DETECTION IN RETINAL  
IMAGE**

by

Mahjabin Maksud

MASTER OF SCIENCE IN ELECTRICAL AND ELECTRONIC ENGINEERING

Department of Electrical and Electronic Engineering  
BANGLADESH UNIVERSITY OF ENGINEERING AND TECHNOLOGY

August 2013

The thesis entitled “**A SPATIAL ENHANCEMENT SCHEME WITH SUPERVISED PIXEL CLASSIFICATION FOR BLOOD VESSEL DETECTION IN RETINAL IMAGE**” submitted by Mahjabin Maksud, Student No.: 0411062275F, Session: April, 2011 has been accepted as satisfactory in partial fulfillment of the requirement for the degree of MASTER OF SCIENCE IN ELECTRICAL AND ELECTRONIC ENGINEERING on August 3, 2013.

### BOARD OF EXAMINERS

1. \_\_\_\_\_  
(Dr. Shaikh Anowarul Fattah) **Chairman**  
*Associate Professor* (Supervisor)  
Department of Electrical and Electronic Engineering  
Bangladesh University of Engineering and Technology  
Dhaka - 1000, Bangladesh.
  
2. \_\_\_\_\_  
(Dr. Pran Kanai Saha) **Member**  
*Professor and Head* (Ex-officio)  
Department of Electrical and Electronic Engineering  
Bangladesh University of Engineering and Technology  
Dhaka - 1000, Bangladesh.
  
3. \_\_\_\_\_  
(Dr. Mohammed Imamul Hassan Bhuiyan) **Member**  
*Associate Professor*  
Department of Electrical and Electronic Engineering  
Bangladesh University of Engineering and Technology  
Dhaka - 1000, Bangladesh.
  
4. \_\_\_\_\_  
(Dr. Mohammad Rakibul Islam ) **Member**  
*Professor* (External)  
Department of Electrical and Electronic Engineering  
Islamic University of Technology (IUT), Bangladesh  
Board Bazar, Gazipur-1704, Bangladesh.

## CANDIDATE'S DECLARATION

I, do, hereby declare that neither this thesis nor any part of it has been submitted elsewhere for the award of any degree or diploma.

Signature of the Candidate

---

Mahjabin Maksud

# Dedication

*To my parents.*

# Acknowledgments

I would like to express my unbound respect and thankfulness to my supervisor Dr. Shaikh Anowarul Fattah for his proper guidance and support during the span of this research. I worked under his supervision even during my undergraduate studies. My interest towards research first flourished in the final year of undergraduate program, whilst I went to work for him. It was him who motivated me to incite my own aptitude for knowing the unknown, encouraged me to the utmost and gave rise to the confidence in me that in an underdeveloped country like ours; it is possible to conduct research of superior quality even in the undergraduate level. He not only acted as my supervisor, but also helped me take important decisions of my academic career. Among many things I learned from Dr. Fattah, perseverance and constant hard work are the keys to open doors of solutions for several important issues in the area of Retinal Blood Vessel Detection. I believe our work in the past one year advanced the state of art of the blood vessels detection and classification problem. I also want to thank him for affording so much time for me in exploring new areas of my research and new ideas and improving the writing of this dissertation. Then I would like to thank Mr. Shubhro Aich who helped me enormously to develop the idea of vessel candidate selection and employ it properly in my classification scheme of vessel pixels. I would also like to thank the rest of the members of my thesis committee: Prof. Dr. Pran Kanai Saha, Dr. Mohammed Imamul Hassan Bhuiyan, and Prof. Dr. Mohammad Rakibul Islam, for their encouragement and insightful comments. I would like to thank the head of the department of Electrical and Electronic Engineering for allowing me to use the lab facilities, which contributed greatly in completing the work in time. I wish to give a special thanks to Dr. Celia Shahnaz, for providing inspiration and guidance to walk the right path of research to success during not only MS studies but also the whole span of my research life in BUET. And most importantly, I wish to thank my parents, without whose prayers and constant support, I could never reach this stage of my life.

# Abstract

Retinal blood vessel segmentation is significant in proper detection of vascular anomalies manifested in different retinal pathologies. Perfect knowledge on blood vessel location is necessary for automated detection of retinal diseases. However, accurate identification of blood vessel locations by eye inspection is extremely difficult especially in faded regions or very thin vessel regions. In this thesis, a two-stage automatic vessel detection algorithm is proposed which involves rule based candidate vessel selection algorithm at the first stage followed by a post-processing scheme and a supervised classification algorithm in the second stage. In order to obtain enhanced vessel region, in the preprocessing scheme, first, spatial adaptive median filtering is introduced which can reduce noise generated by nonhomogeneous background and then the morphological Top-Hat transform is used for further background homogenization for vessel enhancement. A gradient based k-neighborhood (for  $k=1, 2, 3$ ) bidirectional spatial search method is proposed to select vessel candidates from preprocessed green plane of retinal image. A post-processing scheme based on spatial similarity and connectivity is employed to finalize the vessel candidate selection. Instead of pixel by pixel classification of the whole retinal image, a supervised classification scheme is developed where only some critical candidate pixels are tested using linear discriminant based classifier. The idea of such a selective classification offers huge computational savings. For feature extraction, both spatial and spectral features of the subregion centered on test pixel and 8-connected spatially shifted subregions with respect to the center pixel are considered. Since feature extraction is carried out on a larger block in comparison to the gradient search operation, in the preprocessing scheme, sequential morphological opening (filtering) operation in Top-Hat transform and background homogenization via shade correction are included. In supervised classification, instead of selecting training pixels by eye inspection, universal trainer selection algorithm is proposed based on principle of connectivity which is verified by discriminating feature characteristics obtained by selected pixels. Extensive simulation is carried out on some retinal image databases and it is found that a satisfactory performance is obtained by using the algorithm.

# Contents

<b>Dedication</b>	<b>iii</b>
<b>Acknowledgements</b>	<b>iv</b>
<b>Abstract</b>	<b>v</b>
<b>1 Introduction</b>	<b>1</b>
1.1 Background . . . . .	1
1.1.1 Retinal Image of Human Eye . . . . .	1
1.1.2 Vessels in Retinal Image . . . . .	3
1.1.3 Eye Diseases Causing Retinal Damage . . . . .	4
1.1.4 Different Types of Diabetic retinopathy . . . . .	5
1.1.5 Literature Review . . . . .	7
<b>2 Proposed Gradient Search Based Vessel Detection Method</b>	<b>12</b>
2.1 Preprocessing . . . . .	12
2.1.1 Image Plane Selection . . . . .	12
2.1.2 Region of Interest Computation . . . . .	13
2.1.3 Vessel Enhancement Using Repetitive Median Filtering . . . . .	14
2.1.4 Vessel Enhancement Using Adaptive Median Filtering . . . . .	16
2.1.5 Vessel Enhancement Using Top-Hat Transform . . . . .	19
2.2 Proposed Gradient Based Search for Vessel Pixel Detection . . . . .	21
2.3 Postprocessing . . . . .	24
2.4 Database Description . . . . .	25
2.5 Results and Analysis . . . . .	26
2.5.1 Comparison to Other Methods . . . . .	29
2.5.2 Processing Times . . . . .	31

2.6	Conclusion . . . . .	32
<b>3</b>	<b>Proposed Vessel Pixel Classification Scheme</b>	<b>39</b>
3.1	Preprocessing . . . . .	40
3.1.1	Background Homogenization based on Shade Correction . . .	41
3.1.2	Vessel Enhancement by Sequential Opening Filtering and Top- Hat Transform . . . . .	42
3.2	Feature Extraction . . . . .	46
3.2.1	Spatial intensity based features . . . . .	46
3.2.2	Spectral Features . . . . .	53
3.2.3	Choice of Spatial Block Size . . . . .	57
3.2.4	Feature Quality . . . . .	57
3.3	Train Formation . . . . .	60
3.3.1	Conventional Manual Approach . . . . .	60
3.3.2	Proposed Connectivity Based Train Set Design . . . . .	60
3.3.3	Train Image Selection . . . . .	64
3.4	Classification . . . . .	64
3.4.1	Linear Discriminant Based Classifier (LDA) . . . . .	64
3.5	Results and Analysis . . . . .	65
3.5.1	Performance Evaluation . . . . .	66
3.5.2	Comparison to Other Methods . . . . .	71
3.5.3	Processing Times . . . . .	72
3.6	Conclusion . . . . .	73
<b>4</b>	<b>Conclusion</b>	<b>76</b>
4.1	Contribution of this Thesis . . . . .	76
4.2	Scope and Future Work . . . . .	78



# List of Tables

2.1	Definition of some parameters to be used in performance metrics . . .	26
2.2	Performance metrics obtained by using the proposed method on DRIVE database images with repetitive median filtering and $N_p = 5$ . . . . .	28
2.3	Performance metrics obtained by using the proposed method on DRIVE database images with adaptive median filtering and $N_p = 5$ . . . . .	29
2.4	Performance metrics obtained by using the proposed method on STARE database images with adaptive median filtering and $N_p = 5$ . . . . .	30
2.5	Performance metrics obtained by using the proposed method on DRIVE database images with adaptive median filtering and $N_p = 3$ . . . . .	31
2.6	Performance metrics obtained by using the proposed method on STARE database images with adaptive median filtering and $N_p = 3$ . . . . .	32
2.7	Performance Metrics Compared To Other Methods On The Stare And Drive Databases In Terms Of Average Accuracy . . . . .	32
2.8	Time requirements by different vessel detection algorithms. Here, Impl=Implementation, M=MATLAB . . . . .	33
3.1	Definition of some spatial features in Mathematical terms . . . . .	47
3.2	Performance metrics obtained by using the proposed method on DRIVE database . . . . .	67
3.3	Performance metrics obtained by using the proposed method on STARE database . . . . .	68
3.4	Performance metrics obtained by using the proposed method on DRIVE database for critical pixel classification . . . . .	69
3.5	Performance metrics obtained by using the proposed method on STARE database for critical pixel classification . . . . .	70

3.6	Comparison between gradient based search method and vessel pixel classification . . . . .	70
3.7	Comparison Among Different Classification Methods In Terms Of Accuracy . . . . .	71
3.8	Performance Metrics Compared To Other Methods On The Stare And Drive Databases In Terms Of Average Accuracy . . . . .	71
3.9	Time requirements by different vessel detection algorithms. Here, Impl=Implementation, M=MATLAB . . . . .	72

# List of Figures

1.1	A view of the retina seen through an ophthalmoscope . . . . .	2
1.2	A section through human eye with a schematic enlargement of the retina . . . . .	2
1.3	A view of the retina of a patient with advanced Glaucoma . . . . .	4
1.4	A view of the retina of a patient with Retinitis pigmentosa . . . . .	5
1.5	A view of the retina of a patient with advanced diabetic retinopathy .	5
1.6	Different types of diabetic retinopathy . . . . .	7
2.1	Two examples of RGB retinal images (one on top, another at bottom). First column: RGB images, Second column: Red plane images, Third column: green plane images, Fourth column: blue plane images . . .	13
2.2	Histograms of intensity values of adaptive median filtered image and original green plane image for both vessel and non-vessel pixels. (a), (c) Pixel intensity of green plane image and (b), (d) pixel intensity of adaptive median filtered image. . . . .	18
2.3	Vessel enhancement obtained by using the proposed preprocessing method based on adaptive median filtering and Top-Hat transform. Top Left: Original green plane image, Top Right: image obtained after adaptive median filtering, Bottom Left: image with central light reflex removal, and Bottom Right: Top-Hat transformed image . . .	21
2.4	Two examples of repetitive median filtering of green plane retinal im- ages (one on top, another at bottom). First Column: Green plane image, Second Column: images obtained after first time median fil- tering, Third Column: images obtained after second time median fil- tering, and Fourth Column: images obtained after third time median filtering, . . . . .	21

2.5	Comparison among output binary images obtained by using the proposed method: (a) ground truth values obtained using the manual labeling by expert, which is available in database, (b)proposed gradient based vessel segmentation with repetitive median filtering, and (c) adaptive median filtering. . . . .	34
2.6	Accuracy plot of Comparison between Gradient Threshold 3 and 5 on DRIVE database. Blue and Green color represent accuracy for Threshold 3 and 5 respectively. . . . .	35
2.7	Accuracy plot of Comparison between Gradient Threshold 3 and 5 on STARE database images. Blue and Green color represent accuracy for Threshold 3 and 5 respectively. . . . .	35
2.8	Comparison among output binary images obtained by using the proposed gradient based search method with different values of neighboring pixel $N_p$ . (a) Manual labeling available in the database, and vessel detection outcome with proposed gradient based threshold for (b) $N_p = 3$ , (c) $N_p = 4$ , and (d) $N_p = 5$ . . . . .	36
2.9	Illustration of the spatial location of classification errors on a DRIVE image. (a) Green plane image, (b) ground truth blood vessels, and (c) detected blood vessels using the proposed method. . . . .	37
2.10	Illustration of the spatial location of classification errors on a STARE image. (a) Green plane image, (b) ground truth blood vessels, and (c) detected blood vessels using the proposed method. . . . .	38
3.1	Shade Corrected Image Formation. (a) Green Plane Image. (b) Background Image. (c) Shade Corrected Image. . . . .	42
3.2	Top Left: Original image, Top Right: Opening, Bottom Left: Closing, Bottom Right: Closing of Bottom Left Figure . . . . .	44
3.3	Sequential Opening Filtering before Top-Hat Transform. Top Left: Shade Corrected Image. Top Right: Complementary Image. Following Images: Sequential Opening Filtering. Bottom Right: Top-Hat Transformed Image . . . . .	45

3.4	Histogram computed for vessel pixels (left figure) and non-vessel pixels (right figure) corresponding to the first spatial statistical feature ( $f_1$ ): difference between the intensity value of the central pixel $I_{VE}(x, y)$ and minimum intensity value of the block $S_{x,y}^\omega$ . . . . .	48
3.5	Histogram computed for vessel pixels (left figure) and non-vessel pixels (right figure) corresponding to the second spatial statistical feature ( $f_2$ ): difference between the intensity value of the central pixel $I_{VE}(x, y)$ and maximum intensity value of the block $S_{x,y}^\omega$ . . . . .	49
3.6	Histogram computed for vessel pixels (left figure) and non-vessel pixels (right figure) corresponding to the third spatial statistical feature ( $f_3$ ): difference between the intensity value of the central pixel $I_{VE}(x, y)$ and average intensity of the block $S_{x,y}^\omega$ . . . . .	49
3.7	Histogram computed for vessel pixels (left figure) and non-vessel pixels (right figure) corresponding to the fourth spatial statistical feature ( $f_4$ ): standard deviation of the pixel intensities of a block $S_{x,y}^\omega$ . . . . .	50
3.8	Histogram computed for vessel pixels (left figure) and non-vessel pixels (right figure) corresponding to the fifth spatial statistical feature ( $f_5$ ): intensity of the candidate pixel. . . . .	51
3.9	Location of blocks on which spatially shifted features are computed. Here, 13 no pixel and pink colored block represent pixel to be tested and the block around it respectively. Isolated block depicts the position of center pixel of each shifted block with respect to the test pixel. . . . .	52
3.10	Histograms computed for vessel pixels (left figure) and non-vessel pixels (right figure) of all shifted blocks. Mean (top figure) and median (bottom figure) of spatially shifted feature values corresponding to the first feature ( $f_1$ ). . . . .	53
3.11	Histograms computed for vessel pixels (left figure) and non-vessel pixels (right figure) of all shifted blocks. Mean (top figure) and median (bottom figure) of spatially shifted feature values corresponding to the second feature ( $f_2$ ). . . . .	53

3.12	Histograms computed for vessel pixels (left figure) and non-vessel pixels (right figure) of all shifted blocks. Mean (top figure) and median (bottom figure) of spatially shifted feature values corresponding to the third feature ( $f_3$ ).	54
3.13	Histograms computed for vessel pixels (left figure) and non-vessel pixels (right figure) of all shifted blocks. Mean (top figure) and median (bottom figure) of spatially shifted feature values corresponding to the fourth feature ( $f_4$ ).	54
3.14	Histograms computed for vessel pixels (left figure) and non-vessel pixels (right figure) of all shifted blocks. Mean (top figure) and median (bottom figure) of spatially shifted feature values corresponding to the fifth feature ( $f_5$ ).	55
3.15	Histograms computed for vessel pixels (left figure) and non-vessel pixels (right figure) corresponding to the first DCT coefficient of the block.	56
3.16	Histograms computed for vessel pixels (left figure) and non-vessel pixels (right figure) corresponding to the second DCT coefficient of the block.	56
3.17	Histograms computed for vessel pixels (left figure) and non-vessel pixels (right figure) corresponding to the third DCT coefficient of the block.	56
3.18	Histograms computed for vessel pixels (left figure) and non-vessel pixels (right figure) corresponding to the first DCT coefficient of the block.	57
3.19	Within Class Compactness. X-axis Dimension: (1)-(5) Five Spatial Features. Blue and green color refer to vessel and nonvessel pixels respectively.	58
3.20	Within Class Compactness. X-axis Dimension: (1)-(5) Average of Five Spatially Shifted Statistical Features. Blue and green color refer to vessel and nonvessel pixels respectively.	58

3.21	Within Class Compactness. X-axis Dimension: (1)-(5) Median of Five Spatially Shifted Statistical Features. Blue and green color refer to vessel and nonvessel pixels respectively. . . . .	58
3.22	Between Class Separability. X-axis Dimension: (1)-(5) Centroid of Five Spatial Features. Blue and green color refer to vessel and non-vessel pixels respectively. . . . .	59
3.23	Between Class Separability. X-axis Dimension: (1)-(5) Centroid of Average of Five Spatially Shifted Statistical Features. Blue and green color refer to vessel and nonvessel pixels respectively. . . . .	59
3.24	Between Class Separability. X-axis Dimension: (1)-(5) Centroid of Median of Five Spatially Shifted Statistical Features. Blue and green color refer to vessel and nonvessel pixels respectively. . . . .	59
3.25	Selected pixel types. (a) Strong vessel, (b) less strong vessel, (c) weak vessel, (d) less weak nonvessel, and (e) weak non-vessel. Pixel selection criteria: blue and white color indicate vessel and nonvessel pixels respectively. Dark blue and ash colored pixels indicate vessel and nonvessel center pixel accordingly. . . . .	62
3.26	An example of binary output image of classification. (a) Manual labeling, (b) search output, (c) all candidate classification output and (d) critical candidate classification output . . . . .	74
3.27	Effect of feature dimension reduction on a Particular Image. X-axis Dimension: 1) 2-D DCT Coefficients 2) 5 Spatial Features 3) Proposed Spatial and Shifted Spatial Features 4) All considered Features.	75

# Chapter 1

## Introduction

### 1.1 Background

The human retina is the innermost layer of eye, which looks like a circular disc with a diameter between 30 and 40 mm. With the help of an ophthalmoscope, one can see the retinal image of human eye as shown in Fig. 1.1. The examiner sees the neurosensory retina against the background orange color of the melanin containing retinal pigment epithelium and blood-filled choroidal layer of the eye. There are several blood vessels (arteries and veins) within the retina, which ensure continuous blood supply. For normal eyes without any eye diseases, retinal blood vessels exhibit quite regular shape. Different eye diseases cause different types of deformation in retinal vessels, such as blockage, shrinkage and pigmentation. Retinal blood vessel detection plays an important role in proper diagnosis of different retinal diseases caused by extra fluid and blood leakage from damaged vessels. Accurate knowledge on the location of blood vessels can help in reducing the chances of false detection of some retinal diseases [1]- [2]. However, it is extremely difficult for physicians to identify vessel locations from given retinal images by eye inspection, as there are several vessels which are very thin or not very prominent or do not possess sharp edges.

#### 1.1.1 Retinal Image of Human Eye

In Fig. 1.2, a typical cross-section of human eye is shown where along with the retina some major parts are indicated. The eye itself is a mostly hollow organ, roughly spherical in shape. In adults, the eye measures approximately 22 mm in diameter. The walls of the eye consist of the firm outermost coat, white sclera and clear cornea.



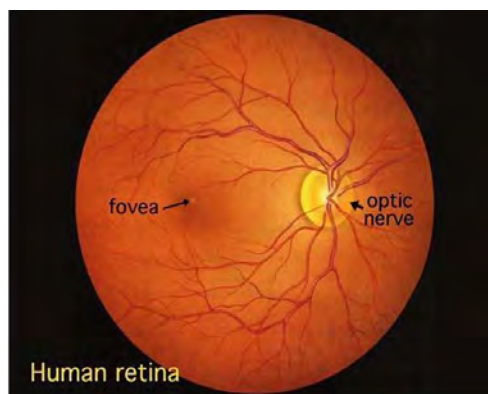


Fig. 1.1: A view of the retina seen through an ophthalmoscope

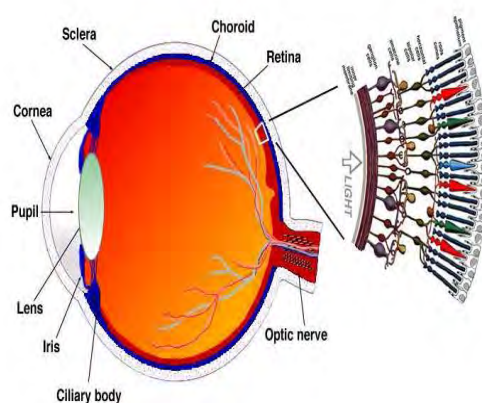


Fig. 1.2: A section through human eye with a schematic enlargement of the retina

The middle layer consists of the uveal tract which is made up of choroid, ciliary body and iris. The human retina is located on the inner surface of the posterior two-thirds to three-quarters of the eye. It is the innermost layer. Assuming that the ocular media (cornea, anterior chamber, and lens) are not cloudy, the living retina can be examined using a direct or indirect ophthalmoscope or a retinal lens at the slit lamp. The retina may also be photographed using a retinal camera. The retina, with the exception of the blood vessels coursing through it, is transparent to the examiner up to its outer layer, the retinal pigment epithelium. The transparent portion of the retina is known as the neurosensory retina.

At the center of the retinal image there is the optic nerve, a circular to oval white area. From the center of the optic nerve major blood vessels are dispersed all

around the retina. Retinal nerve fibers exit the eye through the optic nerve. There is no retinal tissue overlying the optic nerve head or optic disc, which is oval in shape. Beside the optic disc, there is slightly oval-shaped blood vessel-free reddish spot, known as the fovea. A circular field of approximately 6 mm around the fovea is considered the central retina while beyond this is peripheral retina.

### **1.1.2 Vessels in Retinal Image**

The retina at the back of the eye requires a constant blood supply. This blood supply makes sure that the cells of the retina get all the nutrients they need to continue working. The blood supply also removes any waste material that the cells have finished with. Like the rest of the body there are two types of blood vessels concerned with the blood supply to the retina, arteries and veins. Arteries carry the fresh blood from the heart and lungs to all the cells in our bodies. Veins take away the blood that has been used by the cells and return it to the lungs and heart to be refreshed with oxygen and other nutrients. This process happens every time our heart beats so there is a constant stream of fresh blood and nutrients reaching all the cells in our bodies.

#### **Retinal Vessel Occlusion**

A blockage in either a retinal vein or artery is known as ‘retinal vessel occlusion’, which can affect the sight. The main cause of occlusion is atherosclerosis, which makes the blood vessels thinner and sticky. Thus it becomes harder for the blood to flow through it and sticky blood vessels may catch debris in the blood, which in turn can cut off part or all of the blood going to or from the retina. Due to occlusion in retinal arteries, fresh blood cannot enter and retinal cells quickly suffer from the lack of fresh oxygen. This stops them working and sight can be affected quite badly. The amount of sight that is affected varies according to the location of the blockage. On the other hand, due to occlusion in retinal veins, used blood cannot be drained away properly. This can cause the area to swell and may also cause areas of hemorrhage (bleeding). It is to be mentioned that the problem of thinning arteries and veins can cause other problems like heart attacks and strokes.

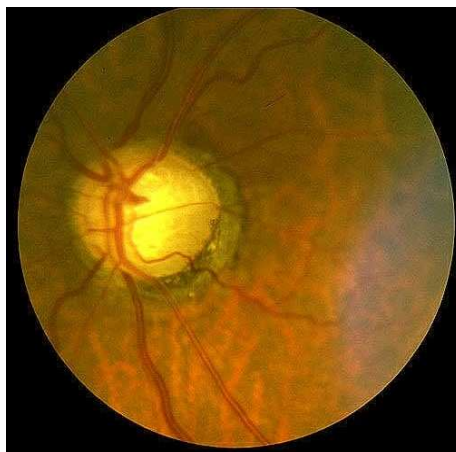


Fig. 1.3: A view of the retina of a patient with advanced Glaucoma

### 1.1.3 Eye Diseases Causing Retinal Damage

Damages in retina due to some eye diseases may lead to serious damage to the nerve cells that carry the vital messages about the visual image to the brain. Three such eye diseases are discussed below.

#### **Glaucoma**

Glaucoma is a common problem in aging, which causes rise in pressure within the eye when anterior chamber of the eye cannot exchange fluid properly. As a result, some blood vessels of the optic nerve head may be damaged. In Fig. 1.3, a view of the retina of a patient with advanced Glaucoma is shown.

#### **Retinitis pigmentosa**

Retinitis pigmentosa is a hereditary disease of the retina for which there is no cure at present. The rods of the peripheral retina begin to degenerate in early stages of this disease. Patients become night blind gradually and they suffer from tunnel vision. Characteristic pathologies are the occurrence of black pigment in the peripheral retina and thinned blood vessels at the optic nerve head. In Fig. 1.4, a view of the retina of a patient with Retinitis pigmentosa is shown.

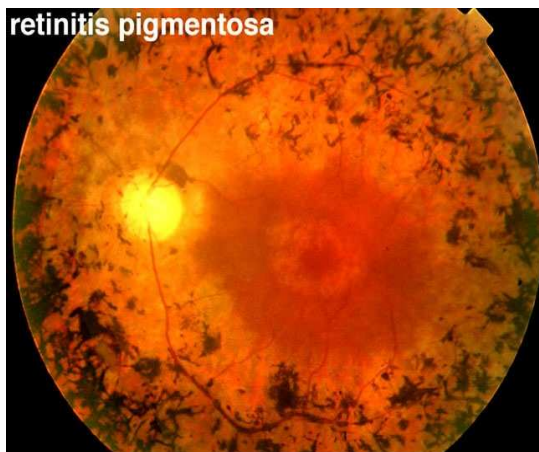


Fig. 1.4: A view of the retina of a patient with Retinitis pigmentosa

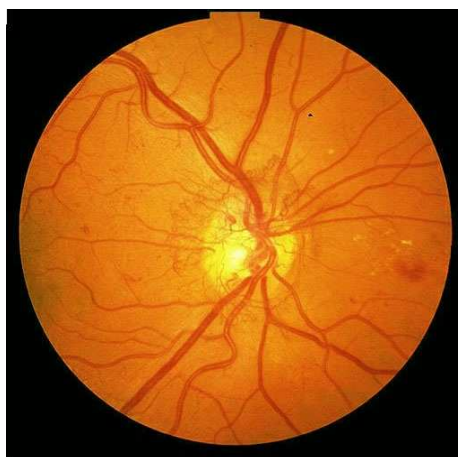


Fig. 1.5: A view of the retina of a patient with advanced diabetic retinopathy

### **Diabetic retinopathy**

Diabetic retinopathy is a side effect of diabetes that affects the retina and can cause blindness. The vital nourishing blood vessels of the eye become distorted and multiplied in uncontrollable ways. In Fig. 1.5, a retinal image of a patient with advanced diabetic retinopathy is shown.

#### **1.1.4 Different Types of Diabetic retinopathy**

Diabetic retinopathy is the result of microvascular retinal changes, which makes the retinal blood vessels become more permeable. There are two types of diabetic retinopathy:

### **Nonproliferative diabetic retinopathy (NPDR)**

It is the earliest stage of diabetic retinopathy. With this condition, damaged blood vessels in the retina begin to leak extra fluids, blood and deposits of cholesterol or other fats. NPDR can cause following changes in the eye:

1. **Microaneurysms:** Small bulges are generated in retinal blood vessels that often leak fluid.
2. **Retinal hemorrhages:** Tiny spots of blood appear, which leak into the retina.
3. **Hard exudates:** Cholesterol or other fats are deposited from the blood that have leaked into the retina.
4. **Macular edema:** Fluid that is leaking from the retina's blood vessels causes swelling or thickening of the macula. Macular edema is the most common cause of vision loss in diabetes.
5. **Macular ischemia:** Small blood vessels become closed, which causes vision blurrin.

### **Proliferative diabetic retinopathy (PDR)**

It mainly occurs when many of the blood vessels in the retina close, preventing enough blood flow. In an attempt to supply blood to the area where the original vessels closed, the retina responds by growing new blood vessels. This is called neovascularization. However, these new blood vessels are abnormal and do not supply the retina with proper blood flow. The new vessels are also often accompanied by scar tissue that may cause the retina to wrinkle or detach. PDR may cause more severe vision loss than NPDR because it can affect both central and peripheral vision. PDR affects vision in the following ways:

1. **Vitreous hemorrhage:** Delicate new blood vessels bleed into the vitreous, the gel in the center of the eye, preventing light rays from reaching the retina.
2. **Traction retinal detachment:** Scar tissue from neovascularization shrinks, causing the retina to wrinkle and pull from its normal position.

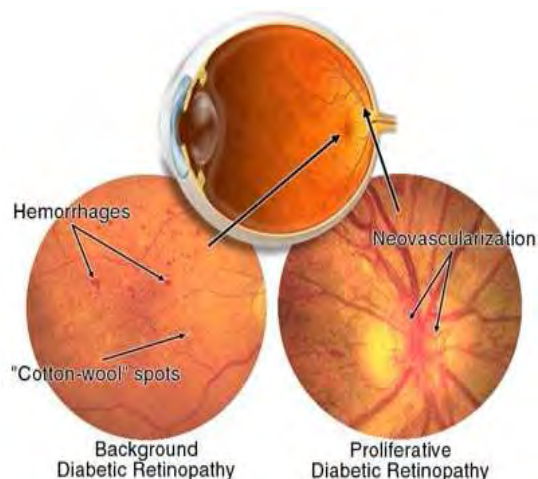


Fig. 1.6: Different types of diabetic retinopathy

3. **Neovascular glaucoma:** If a number of retinal vessels are closed, new blood vessels may block the normal flow of fluid out of the eye. Pressure builds up in the eye, a particularly severe condition that causes damage to the optic nerve.

### 1.1.5 Literature Review

Several methods have been proposed for automatic vessel detection, which in general can be classified into two broad categories, namely rule-based and supervised classification methods. The rule based methods rely on some specific image processing operations and detect vessels from the processed retinal image based on set of predefined rules.

On the other hand, supervised methods utilize some classifiers for pixel classification based on some extracted features.

Among rule-based methods, there are some vessel tracking algorithms which attempt to obtain the vasculature structure by following vessel center lines [3]- [4]. Starting from an initial set of points selected automatically or by manual labeling, vessels are traced by utilizing local information which is obtained from the most appropriate candidate pixel residing in the close neighborhood of the pixel currently under consideration. There are some vessel detection methods based on mathematical morphology [5]- [6]. These methods take benefit from a priori-known vasculature

shape features, such as being piecewise linear and connected. By applying morphological operators, the vasculature is filtered from the background for final segmentation. In matched filter based techniques, usually 2-D linear structural element with a Gaussian cross-profile section, extruded or rotated into three dimensions, is used for blood vessel cross-profile identification (typically a Gaussian or Gaussian-derivative profile) [7]- [8]. The kernel is rotated into many different orientations (usually 8 or 12) to fit into vessels of different configuration. The image is then thresholded to extract the vessel silhouette from the background. There are some model-based vessel detection methods, which employ locally adaptive thresholding. In [9], a general framework using a verification-based multi-threshold probing scheme is proposed, where relevant information related to retinal vessels is incorporated into the verification process. On the other hand, deformable or snake models have been also used for vessel detection in [10] and [11]. A snake is an active contour model that, once placed on the image near the contour of interest, can evolve to fit the shape of the desired structure by an iterative adaption. In [12], a method based on multi-scale feature extraction is proposed. In this method, the local maxima over scales of the gradient magnitude and the maximum principal curvature of the Hessian tensor were used in a multiple pass region growing procedure. Finally the blood vessels are segmented by using both the growth feature and spatial information. In [13], blood vessel-like objects are first extracted by using the Laplacian operator and pruning the noisy objects according to centerlines. Finally vessels are detected by means of normalized gradient vector field. In [14], an unsupervised algorithm is described to detect and measure blood vessels in retinal images. This involves two main steps. The first is an approach for vessel segmentation by thresholding wavelet coefficients. The second step consists of a new alternative to the graph-based algorithm to extract centrelines and localize vessel edges from image profiles, by making use of spline fitting to determine vessel orientations and then searching for the zero-crossings of the second derivative perpendicular to the vessel.

On the other hand, supervised methods are based on pixel classification into two classes, vessel and non-vessel by using different types of classifiers. Classifiers are trained by using supervised learning with data from manually-labeled images. In [15], a back propagation multilayer neural network (NN) is designed for vascular

tree segmentation. Prior to classification, histogram equalization, smoothing and edge detection were carried out on the retinal image and finally dividing the whole image into some small square regions, values of these pixel windows are fed to NN classifier. The method proposed in [16] also utilizes small sub-images centered on the pixel under evaluation in NN classifier. Each pixel in the image is classified by using the first principal component and the edge strength values obtained from the sub-images. In [17], 31-component pixel feature vector is constructed with the Gaussian and its derivatives up to order 2 at 5 different scales and then the k-nearest neighbor (KNN) classifier is employed. The assumption that vessels are elongated structures is the basis for the supervised ridge-based vessel detection method reported in [18]. Ridges are extracted from the image and used as primitives to form line elements. Each pixel is then assigned to its nearest line element, the image thus being partitioned into patches. For every pixel, 27 features are first computed and then a set of reduced features, obtained based on class separability, is employed in KNN classifier. In [19], Gaussian mixture model based Bayesian classifier is used and for feature extraction multi-scale analysis is performed on the image by using the Gabor wavelet transform. The gray-level of the inverted green channel and the maximum Gabor transform response over angles at four different scales are considered as pixel features. In [20], two orthogonal line detectors along with the gray-level of the target pixel are used to construct the feature vector and support vector machine (SVM) classifier is employed for vessel classification. The NN based classification scheme proposed in [21] incorporates a post-processing stage for filling pixel gaps in detected blood vessels and removing falsely-detected isolated vessel pixels. Here for feature extraction the neighborhood of the pixel under consideration from preprocessed retinal images is considered. The preprocessing stage mainly includes gray-level homogenization and blood vessel enhancement.

It is found that in rule-based methods, blood vessels are identified after employing some preprocessing techniques on the retinal image [22]- [23]. Most of these methods are threshold dependent and face problem in detecting weak vessel regions. On the other hand, in case of supervised pixel classification methods, features are extracted from the neighborhood of the desired pixel and different standard classifiers are employed to classify each pixel [15]- [21]. One major drawback of these



pixel level classification schemes is the involvement of huge computational burden since each retinal image under test consists of enormously large number of pixels. Moreover, in all cases, process of selecting the training pixels from a large number of pixels available from train images is based on eye inspection. Finally in both type of vessel detection methods, the preprocessing stage may suffer from providing locations of weak vessel pixels which exhibit confusing characteristics similar to non-vessel pixels. Hence, there is still demand to develop a scheme which utilizes both rule-based and supervised classification methods with necessary modification to overcome the respective limitations and can provide better accuracy in retinal blood vessel detection.

### **Objectives with Specific Aims**

The objectives of this thesis are:

1. To develop a preprocessing scheme for spatial domain enhancement of vessel region.
2. To propose a gradient based method for vessel candidate selection.
3. To design a general rule for selecting train data set consisting of both strong and weak vessel pixels.
4. To extract efficient features based on spatially shifted masks.
5. To reduce computational complexity in pixel based classification.
6. To verify the detection performance on real retinal images utilizing different classifiers.

### **Organization of the Thesis**

The proposed method involves two different approaches for vessel detection: (1) vessel detection based on gradient search on a pre-processed image and (2) pixel level classification of candidate vessels using some robust features.

In Chapter 2, gradient search based vessel detection method is described. Overall there are three major steps involved in this method: preprocessing, gradient based search, and postprocessing. Prior to vessel detection through gradient based search

method, a preprocessing scheme is presented, which offers spatial domain enhancement of vessel region. Here different types of preprocessing methods are discussed. In particular, the background subtraction and median filtering based algorithms are presented in detail. Morphological operators used in the proposed method are then discussed. Next proposed gradient based vessel search algorithm is presented. A postprocessing method is discussed which is applied to obtain better vessel detection accuracy. Finally experimental results on two widely used standard retinal image databases are presented along with comparative performance analysis.

In Chapter 3, the proposed pixel level classification scheme is presented which involves four major tasks, such as critical vessel selection for classification, feature extraction, train data selection, classifier design. First, instead of conventional manual selection approach, a general rule is developed to prepare the train data set consisting of both strong and weak vessel pixels. Next, additional preprocessing stages required for efficient feature extraction are described. Proposed spatial, shifted spatial and spectral features along with some statistical characteristics of extracted features are discussed in detail. Different classifiers tested in the proposed scheme are then presented. Finally experimental results with comparative analysis are demonstrated considering two standard retinal image databases. Chapter 4 summarizes the outcome this thesis with some concluding remarks and possible future works.

## Chapter 2

# Proposed Gradient Search Based Vessel Detection Method

In this chapter, a gradient search based vessel detection algorithm is proposed, which consists of three major steps: pre-processing, gradient based search and post-processing. First the pre-processing stage is demonstrated where we introduce the adaptive median filtering followed by the top hat transform in view of obtaining significant vessel pixel enhancement. Apart from these two techniques, a spatial morphological operation for pre-processing are also described. Next, the proposed gradient based vessel detection algorithm is described in detail, which can identify the edges of a vessel and is capable of distinguishing vessel zones from non-vessel region. Finally a post-processing algorithm is presented, which is incorporated in order to remove falsely detected isolated vessel pixels.

## 2.1 Preprocessing

Color fundus images often exhibit lighting variations, poor contrast, and noise corruption. In order to reduce these imperfections and generate images those are more suitable for distinguishing between vessel and non-vessel pixels in gradient based search method or in feature extraction step of classification based approaches, an efficient preprocessing algorithm is required. In what follows, different steps involved in the preprocessing scheme are described.

### 2.1.1 Image Plane Selection

As a colored picture, the retinal image contains three basic color planes, namely red (R), green (G), and blue (B). One may start processing all three planes for

vessel detection. In Fig. 2.1, RGB retinal image along with images corresponding to single plane, i.e., red plane image, green plane image, and blue plane image are shown. The appearance of vessels in these images is not same and the difference is quite visible by eye inspection. It is well established in literature that when the RGB components of the colored images are visualized separately, the green plane shows the best vessel/background contrast, whereas the red and blue planes show comparatively lower contrast and they are very noisy [24]. Therefore, in the proposed method, only green plane retinal image is considered, which provides better representation of blood vessels and thus computational cost, in comparison to the methods utilizing all three planes, is drastically reduced.

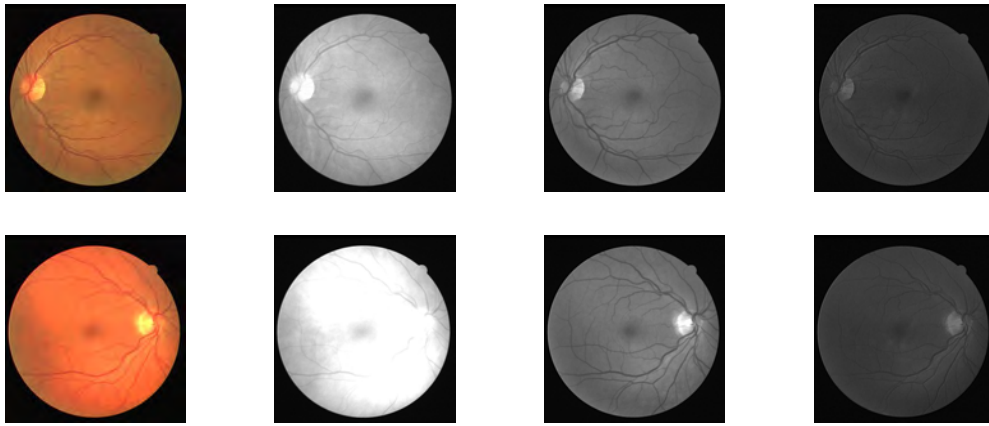


Fig. 2.1: Two examples of RGB retinal images (one on top, another at bottom). First column: RGB images, Second column: Red plane images, Third column: green plane images, Fourth column: blue plane images

### 2.1.2 Region of Interest Computation

In order to remove the strong contrast between the retinal fundus and the region outside the camera aperture, a region of interest (ROI) is specified based on the camera's aperture [19]. Generally, the shape of ROI, like camera's aperture, is circular. The intensity variation pattern outside the ROI is completely different than that of the inner part of the ROI as can be observed from Fig. 2.1 showing a general retinal fundus. The circular pattern matching provides a set of pixels those are residing outside the ROI. In order to precisely obtain the radius of the circle, on the border the neighborhood smoothing is carried out and based on intensity variation between the region residing inside and outside the ROI, radius is adjusted.

For neighborhood smoothing each pixel value of a set of pixels in a subregion is replaced with the mean value of that subregion using eight-neighborhood. Finally, the radius offering the maximum variation is chosen to extract the desired circular ROI.

In the proposed method, for an initial estimate of the diameter of the circle a simple intensity based threshold is used, which helps to discard the region outside the camera apertures. The reason behind relying on this global threshold lies in the facilitation of some computational complexities. It avoids manually drawing the ROI or computationally expensive morphological operations for obtaining the ROI [19]. Note that this global thresholding is not introduced for detecting the vessel pixels, it is just employed to select an approximate ROI. Further processing for ROI detection is explained before. However, such a global threshold is also valid to detect a portion of nonvessel pixels located in the ROI.

### **2.1.3 Vessel Enhancement Using Repetitive Median Filtering**

Retinal fundus photographs often contain an intensity variation in the background across the image, namely “vignetting”, the imbalance primarily due to an optical aberration. Vignetting is the result of an improper focusing of light through an optical system. The result is that the brightness of the image generally decreases radially outward from near the center of the image. A retinal image is captured by viewing the inner rear surface of the eyeball through the pupil. The lens of the camera works in conjunction with the lens of the eyeball to form the image. Since the position of the eye relative to the camera varies from image to image, the exact properties of the vignetting also vary from image to image. Consequently, background pixels may have different intensity for the same image and although their gray-levels are usually higher than those of vessel pixels (in relation to green channel images), the intensity values of some background pixels are comparable to those of brighter vessel pixels. This effect can deteriorate the performance of the vessel detection system.

There are several approaches available in literature to perform vessel enhancement [1], [25], [26]. In [1], a shade correction algorithm is used to obtain vessel enhancement. An estimate of the background image is first computed by median

filtering the original green plane image. Then the background image is subtracted from the original green plane image to obtain “shade corrected” image. The size of the median filter was chosen  $25 \times 25$  pixel such that it is wider than the widest blood vessel, generally appear in the dataset of retinal images. To overcome vignetting and other forms of uneven illumination, in [25], each pixel intensity value is adjusted by adding an amount which is the difference between the desired average intensity (128 in an 8-bit grayscale image) and the mean intensity value of the pixels within a window of size  $N \times N$  with  $N = 40$ . In [26], on top of such adjustment, an adaptive histogram equalization (AHE) is employed in order to normalize and enhance the contrast within fundus images found to be especially effective in detecting small blood vessels characterized by low contrast levels. The AHE is applied to an intensity adjusted inverted green plane image where each pixel  $p$  is adapted using the following formula

$$I_{AHE}(p) = \left( \sum_{p' \in R(p)} \frac{s(I(p) - I(p'))}{h^2} \right)^r * M, \quad (2.1)$$

where  $M = 255$ ,  $R(p)$  denotes the pixel  $p$ 's neighborhood (a square window with length  $h$ ),  $s(d) = 1$  if  $d > 0$ , and  $s(d) = 0$  otherwise. The values of  $h$  and  $r$  were empirically chosen by [27] to be 81 and 8.

In the proposed vessel detection method, in order to perform vessel enhancement, median filtering based algorithms are utilized. In this subsection, the repeated median filtering based vessel enhancement algorithm proposed in this research is introduced. In the next subsection, we introduce the adaptive median filtering based vessel enhancement algorithm.

The median filter is normally used to reduce noise in an image, somewhat like the mean filter. However, it often does a better job than the mean filter by preserving useful details in the image. The median filter belongs to the class of edge preserving smoothing filters those are non-linear filters. This filter smooths the data while keeping the small and sharp details. The median is just the middle value of all the values of the pixels in the neighborhood. The median is a stronger “central indicator” than the mean (or average). In particular, the median is hardly affected by a small number of discrepant values among the pixels in the neighborhood. Consequently, median filtering is very effective at removing various kinds of noise, in particular the “salt and pepper” noise, a very common noise corrupting the retinal image. A

median filter is more effective than convolution when the goal is to simultaneously reduce noise and preserve edges. In [28], it is shown that initial median filtering can remove small dark spots, while leaving the rest of the image approximately unchanged.

Like the mean filter, the median filter considers each pixel in the image in turn and looks at its nearby neighbors to decide whether or not it is representative of its surroundings. Instead of simply replacing the pixel value with the mean of neighboring pixel values, it replaces it with the median of those values. The median is calculated by first sorting all the pixel values from the surrounding neighborhood into numerical order and then replacing the pixel being considered with the middle pixel value. (If the neighborhood under consideration contains an even number of pixels, the average of the two middle pixel values is used.) The median filter is a non-linear tool, while the average filter is a linear one. In smooth, uniform areas of the image, the median and the average will differ by very little. The median filter removes noise, while the average filter just spreads it around evenly. The performance of median filter is particularly better for removing impulse noise than average filter. In this research, median filtering is performed on several retinal images and the effect is analyzed. It is found that an image after performing the median filtering may still contain noise. Since median filtering is edge preserving operation which smooths the data while keeping the small and sharp details, the median filtering operation is performed again on that image. As expected that a further noise reduction is achieved resulting in enhanced vessel pixels. One may consider repeating the median filtering operation several times, which not only increases the computational burden, but also deteriorates the vessel edge representation because of over smoothing effect. Hence, performing median filtering operation is restricted to three times, which is experimentally found to be sufficient to provide acceptable level of noise reduction.

#### **2.1.4 Vessel Enhancement Using Adaptive Median Filtering**

Although median filtering is a useful non-linear image smoothing and enhancement technique, it may not always precisely discriminate noise and the fine detail of the image. In many cases, it may remove both the noise and the fine detail of

a retinal image, since it is very difficult to differentiate between the two in this particular application. Anything relatively small in size compared to the size of the neighborhood will have minimal effect on the value of the median and will be filtered out. In other words, the median filter may fail to distinguish fine detail from the noise. As an alternate to the median filtering, in this research, adaptive median filtering is introduced for obtaining better vessel enhancement through significant noise reduction. The adaptive median filter performs spatial processing to determine which pixels in an image have been affected by noise [29]. It classifies pixels as noise by comparing each pixel in the image to its surrounding neighbor pixels. The size of the neighborhood is adjustable, as well as the threshold for the comparison. A pixel that is different from a majority of its neighbors, as well as being not structurally aligned with those pixels to which it is similar, is labeled as noise pixel. These noise pixels are then replaced by the median pixel value of the pixels in the neighborhood that have passed the noise labeling test. The median filter performs well as long as the spatial density of the noise is not large. However the adaptive median filtering can handle noise with probabilities even larger than these. An additional benefit of the adaptive median filter is that it seeks to preserve detail while performing overall smoothing operation on the image. Considering the high level of noise, the adaptive algorithm performs quite well.

Purposes of adaptive median filtering are:

- Removal of impulse noise
- Smoothing of other noise
- Reduction in distortion, like excessive thinning or thickening of object boundaries

### **Working Procedure of Adaptive Median Filtering**

Adaptive median filter changes size of  $S_{xy}$  (the size of the neighborhood) during operation. Here,

$Z_{min}$  = minimum gray level value in  $S_{xy}$

$Z_{max}$  = maximum gray level value in  $S_{xy}$

$Z_{med}$  = median of gray levels in  $S_{xy}$



$Z_{xy}$  = gray level at coordinates (x, y)

$S_{max}$  = maximum allowed size of  $S_{xy}$

---

**Algorithm 1** Algorithm of Adaptive Median Filtering

---

$A1 = Z_{med} - Z_{min}$

$A2 = Z_{med} - Z_{max}$

**if**  $A1 > 0$  AND  $A2 < 0$  **then**

$B1 = Z_{xy} - Z_{min}$

$B2 = Z_{xy} - Z_{max}$

**if**  $B1 > 0$  AND  $B2 < 0$  **then**

$output = Z_{xy}$

**else**

$output = Z_{med}$

**end if**

**else**

Increase the *window size*

**if** *window size*  $< S_{max}$  **then**

Repeat Level A

**else**

$output = Z_{xy}$

**end if**

**end if**

---

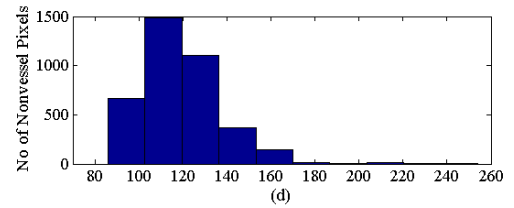
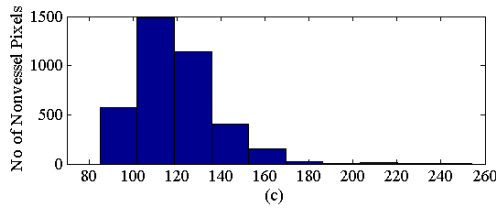
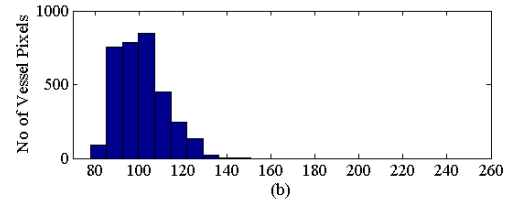
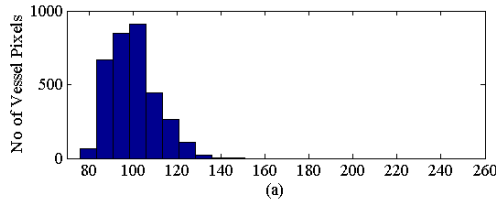


Fig. 2.2: Histograms of intensity values of adaptive median filtered image and original green plane image for both vessel and non-vessel pixels. (a), (c) Pixel intensity of green plane image and (b), (d) pixel intensity of adaptive median filtered image.

In order to demonstrate the effect of adaptive median filtering, in Fig. 2.2, histograms of intensity values of adaptive median filtered image and original green plane image for both vessel and non-vessel pixels are shown. It is observed from

---

**Algorithm 2** Explanation of Algorithm of Adaptive Median Filtering
 

---

```

if  $Z_{min} < Z_{med} < Z_{max}$  then
   $Z_{med}$  is not an impulse
    if  $Z_{min} < Z_{xy} < Z_{max}$  then
       $Z_{xy}$  is not an impulse
         $output = Z_{xy}$ 
      else
        if  $Z_{xy} = Z_{min}$  OR  $Z_{xy} = Z_{max}$  then
           $output = Z_{med}$ 
        end if
       $Z_{med}$  is not an impulse
    end if
  else
     $Z_{med}$  is an impulse
    (1) the size of the window is increased and
    (2) Second condition is repeated until ...
    (a)  $Z_{med}$  is not an impulse and go to first condition or
    (b)  $S_{max}$  reached:  $output = Z_{xy}$ 
  end if

```

---

this figure that the adaptive median filtering preserves the range of intensity values of non-vessel pixels, but it creates a well dispersion in pixel intensities of vessel pixels. That is, a good number of vessel pixels attain a higher intensity values after being passed through the adaptive median filtering operation. Certainly this helps in making a distinction between thin vessel pixels and non-vessel pixels those were not easily distinguishable before. This criterion definitely improves the performance of any kind of vessel detection algorithm. Therefore, in the proposed method of preprocessing in this chapter, adaptive median filtering is applied with a suitable disk size appropriated for reduction in noise generated by nonhomogeneous background and resulting filtered image is denoted as  $I_F$ .

### 2.1.5 Vessel Enhancement Using Top-Hat Transform

In view of obtaining further enhancement of vessel pixels in filtered image  $I_F$ , in this research, Top-Hat transform based morphological operation is carried out. Subtracting an opened image (i.e. an image being processed using morphological opening operation) from the original image is called Top-Hat Transform. It is well known that the morphological opening operation can remove completely regions of an object, which cannot contain the structuring element, smooth object contours, breaks, thin connections, and can remove thin protrusions. In the proposed scheme, for visual

convenience, the Top-Hat transform operation is performed on the complementary image of  $I_F$ , i.e., the vessel enhanced image  $I_{VE}$  can be expressed as

$$I_{VE} = I_F^C - \gamma(I_F^C) \quad (2.2)$$

where  $\gamma$  is a morphological opening operation using a disc of suitable size. Thus, while bright retinal structures are removed (i.e., optic disc, possible presence of exudates or reflection artifacts), the darker structures remaining after the opening operation become enhanced (i.e., blood vessels, fovea, possible presence of microaneurysms or hemorrhages). Next with the filtered image  $I_F$ , we propose to employ the Top-Hat transformation on  $I_F^C$ .

In this research, different types of preprocessing methods described above have been extensively tested on green plane image. However, it is already explained that adaptive median filtering based preprocessing offers advantages over the repetitive median filtering. Thus, in the proposed vessel detection algorithm, adaptive median filtering along with the Top-Hat transform operation is used for vessel enhancement. The key steps involved in this scheme are summarized below.

1. Adaptive median filtering.
2. Central light reflex removal by applying a morphological opening operation using a three-pixel diameter disc, defined in a square grid by using eight-connectivity, as structuring element.
3. Top-Hat transform with morphological opening operation.

In Fig. 2.3, resultant images obtained by using the above steps are shown.

For the purpose of comparison, effect of using repetitive median filtering based vessel enhancement scheme is shown in Fig. 2.4. In this case, repetitive median filtering operation is performed on green plane image.

The effect of vessel enhancement in these figures may not be visible by eye inspection. In the result section of this chapter, results obtained from images preprocessed in both methods are shown and their efficiencies are compared, which clearly demonstrate the advantage of using the adaptive median filtering based method and the reasons behind have already explained.

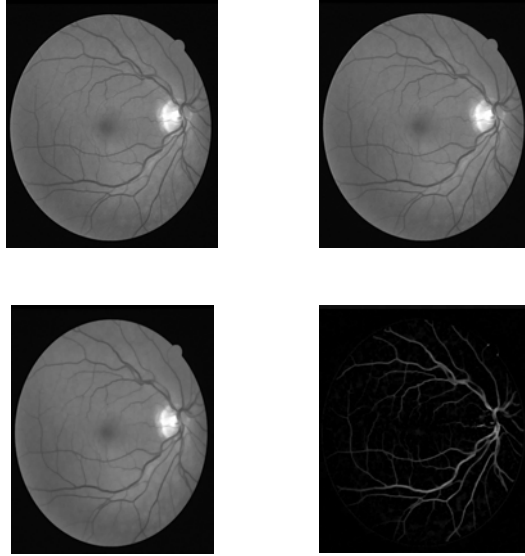


Fig. 2.3: Vessel enhancement obtained by using the proposed preprocessing method based on adaptive median filtering and Top-Hat transform. Top Left: Original green plane image, Top Right: image obtained after adaptive median filtering, Bottom Left: image with central light reflex removal, and Bottom Right: Top-Hat transformed image

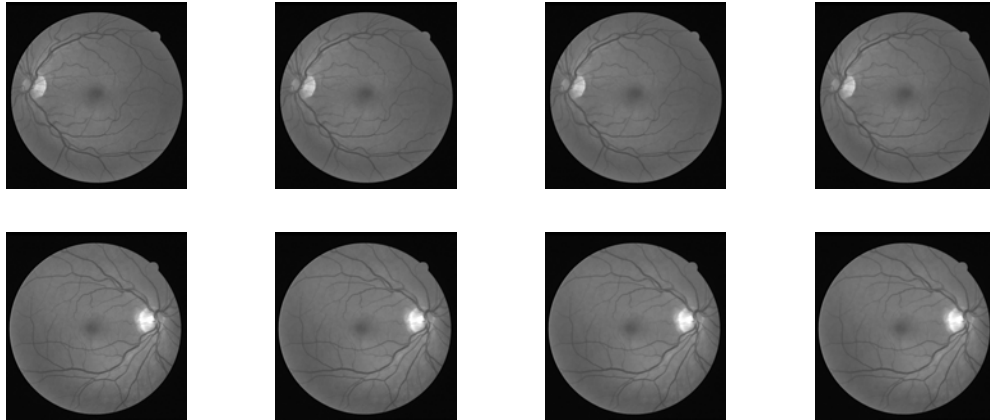


Fig. 2.4: Two examples of repetitive median filtering of green plane retinal images (one on top, another at bottom). First Column: Green plane image, Second Column: images obtained after first time median filtering, Third Column: images obtained after second time median filtering, and Fourth Column: images obtained after third time median filtering,

## 2.2 Proposed Gradient Based Search for Vessel Pixel Detection

From the preprocessed image the objective is now to extract the vessel pixels. It is quite similar to the task of image segmentation which is an important and fun-

damental task in many digital image processing systems. One simple but widely used approach is to perform image segmentation by thresholding, which involves the basic assumption that the foreground (object) of interest and the background in the digital image have distinct intensity distributions. If this assumption holds, the histogram of intensity levels of the image under consideration will contain two or more distinct peaks and a suitable threshold value can be obtained to separate the desired object from the background. The regions (or pixels) having intensity levels below the threshold are assigned to the background and those having the intensity levels above the threshold are assigned to the objects, or vice versa. Threshold selection methods can be classified into two groups, namely, global methods and local methods. A global thresholding technique thresholds the entire image with a single threshold value obtained by using the gray level histogram (which is an approximation of the gray level probability density function) of the image. Local thresholding methods partition the given image into a number of subimages and determine a threshold for each of the subimages. Global thresholding methods are easy to implement and are computationally less involved. Depending on the application, threshold may be adaptively change in different spatial blocks or some knowledge-guided adaptive thresholding can be used [9].

In order to classify the retinal pixels into two class: vessel and non-vessel, in this section, a gradient based neighborhood intensity search algorithm is developed, which is performed on the complementary image of the green plane image preprocessed according to the methods discussed in previous section. For strong and wide vessels, even by eye inspection the variation in the pixel intensity with respect to the background can easily be identified from the enhanced retinal images. However, this is not always true for vessels those are thin and not very prominent. The identification is extremely difficult in vessel edges and tiny vessel branches. The neighborhood intensity gradient of the image matrix is calculated in two mutually orthogonal directions: horizontal and vertical. However for each of these two cases, a bidirectional operation is performed, i.e., for horizontal gradients, row-wise both from left to right and right to left and for vertical gradients, both from top to bottom and from bottom to top are considered. Each of these four directional gradient calculation is performed independently with respect to each other.

It is obvious that the computational burden will be increased due to the computation of these four directional gradient. However, considering the various possible directional patterns of retinal vessels, these operations are extremely useful to precisely capture all possible vessel pixels. Moreover, as the gradient calculation in row wise (or column wise) data can simply be performed by using sample value differences, the computation would not be very high. The intensity value of the pixel under consideration, is compared with those of  $k$  ( $k=1,2,3$ ) neighborhood consecutive pixels along with the previous pixel, and if the difference exceeds a definite threshold in each case, depending on the polarity of the difference, the pixel as well as the neighboring pixel, is declared as vessel or nonvessel. This parameter strongly depends on the width of the vessel on the search path and the maximum number of  $k$  is found to be optimum at 3. The gradient at the edge of a vessel,  $N_p$  is also varied to investigate the performance variation in terms of vessel detection. Considering a very small value of  $N_p$ , say  $N_p = 1$  or  $N_p = 2$  will unnecessarily select large number of pixels and large value of  $N_p$ , say  $N_p > 5$  may not be appropriate considering the common width of vessels appearing on the search path. Hence, in the proposed method,  $N_p$  is restricted between 3 to 5. Instead of considering a single row (or column), multiple rows (or columns) are also considered to analyze subregion based variation for vessel detection. However, considering the thin vessels and vessel edges, it is critical to ascertain the width of the subregion and it is observed that in different portions of the image different widths provide satisfactory performance. Hence, in the proposed scheme single row or column is considered in gradient search, which ensures capturing the variation even for thin vessels of vessel edges.

The gradient based search algorithm can be summarized as follows (considering the case of horizontal left to right search).

$$\begin{aligned} diff &= fig(i, j) - fig(i, j + m) \\ diff1 &= fig(i, j - 1) - fig(i, j) \end{aligned} \quad (2.3)$$

Here,  $\theta = Threshold$  and  $(i, j)$  and  $(i, j + m)$  are the coordinates of the pixel to be labeled and the neighboring pixel respectively and  $m = \text{pixel difference} = 1, 2, 3$ . The outcome of the gradient based scheme is a binary image ascribing '0' to nonvessel pixels and '255' to vessel ones. Similar algorithm is followed in each case of vertical top to bottom and bottom to top search as well as horizontal right to left search.

---

**Algorithm 3** Condition of declaring a pixel as vessel or nonvessel

---

```

if  $diff > \theta+$  then
     $fig(i, j + m) = VesselPixel$ 
     $fig(i, j) = NonvesselPixel$ 
else if  $diff < \theta-$  then
     $fig(i, j) = VesselPixel$ 
else if  $diff1 > \theta+$  then
     $fig(i, j + m) = VesselPixel$ 
     $fig(i, j) = VesselPixel$ 
else if  $diff1 < \theta-$  then
     $fig(i, j) = NonvesselPixel$ 
end if

```

---

A combined binary image found from four searches is declared as the final outcome with marked vessel pixels.

## 2.3 Postprocessing

Gradient based vessel detection algorithm described in the previous subsection, provides a black and white image which, apart from the desired vessel pixels, may contain some isolate single or group of vessel pixels. It is most likely that small isolated regions are misclassified as blood vessel pixels. However some of them could be original vessel pixels appearing as isolated pixels because of wrong detection of some vessels (located in between that isolated zone and correctly identified neighboring vessel zone) as non-vessels. In order to remove these artifacts, the pixel area in each connected region is measured. In artifact removal, each region connected to an area below 50 is reclassified as nonvessel. Apart from this, following morphological operations are carried out to eliminate falsely identified vessel as well as non-vessel pixels:

1. Adjusting the isolated interior pixels of a square block. For example, a single non-vessel pixel residing within a three-by-three block of vessel pixels or a single vessel pixel residing within a three-by-three block of non-vessel pixels.
2. Defining a pixel to vessel if majority (five or more) of the pixels in its three-by-three neighborhood are vessel, otherwise defining it as non-vessel.

It is observed that there is a tendency of exhibiting white thin discontinuous white pixel boundary on the edge of the resulting image received after the gradient based

search. However, complications generally arouse from different retinal diseases may not found on the boundary. Hence, depending on the neighborhood intensity gradient, some primarily detected vessel pixels on the boundary (but inside the ROI) are readjusted.

## 2.4 Database Description

To evaluate the vessel segmentation methodology described in the next section, publicly available databases containing retinal images, the DRIVE database (Available: <http://www.isi.uu.nl/Re-search/Databases/DRIVE>), was used. This database have been widely used by other researchers to test their vessel segmentation methodologies since, apart from being public, it provides manual segmentations for performance evaluation. The DRIVE database comprises 40 eye-fundus color images (seven of which present pathology) taken with a Canon CR5 nonmydriatic 3CCD camera with a  $45^\circ$  field-of-view (FOV). Each image was captured at  $768 \times 584$  pixels, 8 bits per color plane and, in spite of being offered in LZW compressed TIFF format, they were originally saved in JPEG format. The database is divided into two sets: a test set and a training set, each of them containing 20 images. The test set provides the corresponding FOV masks for the images, which are circular (approximated diameter of 540 pixels) and two manual segmentations generated by two different specialists for each image. The selection of the first observer is accepted as ground truth and used for algorithm performance evaluation in literature. The training set also includes the FOV masks for the images and a set of manual segmentations made by the first observer.

The STARE database (Available: <http://www.ces.clemson.edu/>), originally collected by Hoover et al. [23], comprises 20 eye-fundus color images (ten of them contain pathology) captured with a TopCon TRV-50 fundus camera at  $35^\circ$  FOV. The images were digitalized to  $700 \times 605$  pixels, 8 bits per color channel and are available in PPM format. The database contains two sets of manual segmentations made by two different observers. Performance is computed with the segmentations of the first observer as ground truth.



Table 2.1: Definition of some parameters to be used in performance metrics

	<b>Vessel Present</b>	<b>Vessel Absent</b>
<b>Vessel detected</b>	True Positive (TP)	False Positive (FP)
<b>Vessel not detected</b>	False Negative (FN)	True Negative (TN)

## 2.5 Results and Analysis

In order to quantify the algorithmic performance of the proposed method on a fundus image, the resulting vessel detection is compared to its corresponding gold-standard image. This image is obtained by manual creation of a vessel mask in which all vessel pixels are set to one and all non-vessel pixels are set to zero. Thus, automated vessel segmentation performance can be assessed. In view of demonstrating the performance of the proposed vessel detection scheme, five conventional performance metrics are utilized, namely sensitivity  $Se$ , specificity  $Sp$ , positive predictive value  $Ppv$ , negative predictive value  $Npv$ , and overall accuracy  $Acc$ . In Table 2.1, four terms are defined in a convincing way, which are necessary to define the metrics. True positive (TP) is the number of vessel pixels detected correctly, that is the pixel detected as vessel is also labeled as vessel in the ground truth. Similarly, true negative (TN) is the number of no-vessel pixels detected correctly, that is the pixel detected as non-vessel is also labeled as non-vessel in the ground truth. On the other hand, false positive (FP) is the number of pixels detected as vessel, which are labeled as non-vessel in the ground truth, i.e., the number of incorrectly detected vessel. Similarly, false negative (FN) is the number of pixels detected as non-vessel, which are labeled as vessel in the ground truth, i.e., the number of incorrectly detected non-vessel. Taking into account the above definitions, the performance metrics can be defined as

$$Se = \frac{TP}{TP + FN} \quad (2.4)$$

$$Sp = \frac{TN}{TN + FP} \quad (2.5)$$

$$Ppv = \frac{TP}{TP + FP} \quad (2.6)$$

$$Npv = \frac{TN}{TN + FN} \quad (2.7)$$

$$Acc = \frac{TP + TN}{TP + FN + TN + FP} \quad (2.8)$$

The metric sensitivity  $Se$  is the rate of correct vessel declaration among all vessel pixels (no matter correctly identified as vessel or wrongly identified as non-vessel, i.e. TP+FN). Similarly the metric specificity  $Sp$  is the rate of correct non-vessel declaration among all non-vessel pixels (TN+FP). The metric positive predictive value  $Ppv$  is the ratio of pixels declared as vessel pixel that are correctly declared. The metric negative predictive value  $Npv$  is the ratio of pixels declared as background pixel that are correctly declared. Finally, overall accuracy  $Acc$  is a global measure providing the ratio of total well-declared pixels. Since the dark background outside the FOV can easily be detected and there is no use of considering the outside region in performance evaluation, the performance metrics are thus conventionally computed for pixels within the FOV only, which is the ROI. For the DRIVE database, the necessary masks for FOV are given. However, for the STARE database a circular disc is first approximated depending on the average size of the given images and the ROI detection scheme explained in this chapter is employed.

In this section, first, all the performance metrics are evaluated for the proposed method in its two different variants, one which involves repeated median filtering and the other one which utilizes adaptive median filtering. The performance of these two variants of the proposed method for each image of the DRIVE database is shown in Tables 2.2 and 2.3, respectively. As discussed previously, in this table, the value of the parameter  $N_p$  in the proposed gradient search method is set to 5.

It is observed from these tables that among the performance metrics, the value of  $Sp$  and  $Ppv$  increases drastically while applying adaptive median filtering instead of repetitive median filtering for each image. However, in that case, the value of  $Se$  decreases slightly, but the overall accuracy improves. In Fig. 2.5(a), a ground truth retinal image with manual labeling available in the database is shown. Corresponding vessel detection outcome obtained by using the proposed method with two different preprocessing techniques, repetitive median filtering and adaptive median filtering is presented in Figs. 2.5(b) and (c), respectively. It is found that the vessel detection achieved by using the adaptive median filtering is better and smoother in comparison to that which utilizes the repeated median filtering. Similar to Table 2.4, the results obtained with the STARE database using the proposed method with adaptive

Table 2.2: Performance metrics obtained by using the proposed method on DRIVE database images with repetitive median filtering and  $N_p = 5$

<b>Image</b>	$Se$	$Sp$	$Ppv$	$Npv$	<i>Acc in percentage</i>
1	0.7766	0.9478	0.6917	0.9657	92.5340
2	0.7609	0.9414	0.6959	0.9572	91.4358
3	0.6508	0.9578	0.7243	0.9415	91.3037
4	0.7175	0.9399	0.6475	0.9558	91.0255
5	0.6391	0.9693	0.7659	0.9448	92.4526
6	0.6364	0.9654	0.7512	0.9417	91.8945
7	0.6974	0.9225	0.5786	0.9523	89.2676
8	0.6299	0.9307	0.5665	0.9459	89.2900
9	0.6308	0.9655	0.7089	0.9516	92.6215
10	0.6810	0.9666	0.7346	0.9572	93.2517
11	0.7013	0.9207	0.5683	0.9539	89.2215
12	0.7067	0.9533	0.6842	0.9578	92.2453
13	0.6694	0.9590	0.7295	0.9461	91.7943
14	0.7482	0.9342	0.6030	0.9652	91.2235
15	0.7539	0.9154	0.5080	0.9698	89.8630
16	0.6837	0.9534	0.6883	0.9524	91.8114
17	0.6819	0.9368	0.6028	0.9544	90.53764
18	0.7495	0.9370	0.6068	0.9665	91.5435
19	0.7963	0.9594	0.7285	0.9718	93.9764
20	0.7129	0.9565	0.6619	0.9654	93.0552

median filtering and  $N_p = 5$  is shown in Table 2.4.

Next, the effect of variation of the number of neighboring pixels ( $N_p$ ) considered in gradient based search algorithm is investigated. In Tables 2.3, 2.5, 2.4, and 2.6, the results with variable  $N_p$  are listed for both DRIVE and STARE databases.

Among the performance metrics, the value of  $Sp$  and  $Ppv$  increases drastically while increasing threshold from 3 to 5 for each image. Though the value of  $Se$  decreases slightly in case of the proposed method, but the overall accuracy improves significantly. In Fig. 2.6 and Fig. 2.7 effect of gradient threshold can clearly be observed on two databases.

In Fig. 2.8, an image from DRIVE database is represented with manual labeling of blood vessels and labeling through gradient based search method applying different values of  $N_p$ . When  $N_p$  is set to 3, most of the both thick and thin vessels appear along with many isolated vessel zones, which using the proposed pro-processing may or may not be eliminated. Increase in the value of  $N_p$  gradually decreases the vessel

Table 2.3: Performance metrics obtained by using the proposed method on DRIVE database images with adaptive median filtering and  $N_p = 5$

<b>Image</b>	$Se$	$Sp$	$Ppv$	$Npv$	$Acc$ in percentage
1	0.7638	0.9688	0.7870	0.9645	94.1946
2	0.7747	0.9685	0.8126	0.9606	93.9472
3	0.6174	0.9836	0.8653	0.9378	93.0256
4	0.7123	0.9785	0.8358	0.9567	94.2982
5	0.6168	0.9868	0.8798	0.9425	93.6568
6	0.5994	0.9870	0.8834	0.9375	93.2299
7	0.6633	0.9721	0.7840	0.9498	93.1222
8	0.5820	0.9802	0.8087	0.9422	93.0157
9	0.6656	0.9790	0.8085	0.9565	94.2208
10	0.6567	0.9825	0.8360	0.9548	94.3607
11	0.6942	0.9687	0.7677	0.9551	93.3121
12	0.6697	0.9801	0.8283	0.9540	94.1280
13	0.6521	0.9803	0.8454	0.9446	93.3780
14	0.7476	0.9633	0.7316	0.9662	93.7894
15	0.7475	0.9576	0.6713	0.9704	93.5772
16	0.7042	0.9760	0.8151	0.9564	94.0398
17	0.6585	0.9801	0.8233	0.9533	94.0474
18	0.7218	0.9710	0.7639	0.9642	94.2415
19	0.7668	0.9815	0.8504	0.9685	95.5697
20	0.6876	0.9788	0.7945	0.9633	94.7720
<i>Avg</i>	0.687	0.9759	0.8096	0.9549	93.9073

diameter and makes it smooth as much as it appears in actual image, but most of the thin vessels disappear (which is obvious in the decrease in  $Se$ ). Overall performance improves with the increase in  $N_p$ . However, as discussed before,  $N_p$  is varied between 3 to 5. In Fig. 2.9 and Fig. 2.10, two images from DRIVE and STARE databases are shown along with the ground truth (manual labeling of blood vessels available in the database) and labeled output image obtained by using the proposed method are shown. It is observed from these figures that the vessels detected by using the proposed scheme closely map the ground truth vessel location except in case of very thin vessels and vessel edges.

### 2.5.1 Comparison to Other Methods

Table 2.7 provides comparison of the performance of the proposed method in terms of average accuracy to other methods. It is observed that the accuracy of the

Table 2.4: Performance metrics obtained by using the proposed method on STARE database images with adaptive median filtering and  $N_p = 5$

<b>Image</b>	$Se$	$Sp$	$Ppv$	$Npv$	<i>Acc in percentage</i>
1	0.5586	0.9697	0.6919	0.9474	92.4991
2	0.6754	0.9645	0.6692	0.9655	93.6723
3	0.7800	0.9343	0.5156	0.9793	92.1622
4	0.4504	0.9881	0.8158	0.9390	93.1914
5	0.7581	0.9419	0.6509	0.9646	91.8961
6	0.8610	0.9454	0.6065	0.9858	93.7922
7	0.8457	0.9385	0.6297	0.9801	92.8283
8	0.8388	0.9530	0.6722	0.9809	94.1214
9	0.8224	0.9534	0.6807	0.9780	93.9233
10	0.7509	0.9450	0.6300	0.9682	92.3537
11	0.8401	0.9591	0.6931	0.9820	94.7360
12	0.9031	0.9482	0.6760	0.9879	94.3398
13	0.8118	0.9596	0.7374	0.9733	94.1532
14	0.8028	0.9607	0.7457	0.9714	94.0878
15	0.7135	0.9720	0.7744	0.9618	94.1255
16	0.5105	0.9840	0.8414	0.9236	91.6457
17	0.7781	0.9737	0.8069	0.9688	94.9435
18	0.6698	0.9892	0.8251	0.9752	96.6638
19	0.6658	0.9813	0.6886	0.9793	96.2894
20	0.6478	0.9676	0.6714	0.9641	93.7939
<i>Avg</i>	0.7342	0.9614	0.7011	0.9688	93.9109

proposed method is comparable with those of other papers. However, the novelty and simplicity of the proposed method is quite noticeable. The simple and vastly competent search algorithm used in the gradient based search method. Accuracy of the proposed method is higher compared to every rule-based method except [6].

[6] employs a complex and lengthy methodology consisting of three consecutive phases, preprocessing applying shade correction and thin vessel enhancement with a set of line detection filters, vessel centerline detection applying Gaussian filters to obtain four directional difference information and a region growing process to obtain connection of the candidate points, and vessel segmentation applying a modified top-hat transform and a binary morphological reconstruction method to obtain binary maps of the vessels and vessel filling. But the novelty and simplicity of the proposed method is simply more considerable even negotiating accuracy slightly.

Table 2.5: Performance metrics obtained by using the proposed method on DRIVE database images with adaptive median filtering and  $N_p = 3$

<b>Image</b>	$Se$	$Sp$	$Ppv$	$Npv$	<i>Acc in percentage</i>
1	0.8664	0.9149	0.6058	0.9784	90.8578
2	0.8601	0.8986	0.5992	0.9733	89.2846
3	0.7716	0.9339	0.6655	0.9600	91.0215
4	0.8016	0.9356	0.6569	0.9684	91.7711
5	0.7398	0.9519	0.7072	0.9588	92.3116
6	0.7309	0.9502	0.7068	0.9555	91.9239
7	0.7775	0.9018	0.5471	0.9637	88.5332
8	0.7466	0.9291	0.6023	0.9623	90.6192
9	0.7344	0.9577	0.6982	0.9644	93.1512
10	0.7733	0.9428	0.6471	0.9684	92.2563
11	0.7940	0.8932	0.5255	0.9668	88.0367
12	0.8008	0.9309	0.6237	0.9703	91.4598
13	0.7833	0.9309	0.6520	0.9630	91.0004
14	0.8522	0.8901	0.5089	0.9783	88.5616
15	0.8430	0.8710	0.4308	0.9795	86.8048
16	0.8327	0.9228	0.6188	0.9734	91.0986
17	0.7847	0.9292	0.6092	0.9684	91.1401
18	0.8446	0.9157	0.5654	0.9785	90.7571
19	0.8763	0.9327	0.6406	0.9822	92.5950
20	0.8415	0.9372	0.6152	0.9802	92.6966
<i>Avg</i>	0.8028	0.9235	0.6479	0.9697	90.7941

## 2.5.2 Processing Times

It is observed that the superiority of the proposed schemes over other algorithms tested using the DRIVE database is in the time requirement to process an image with appreciable accuracy. Computational time for the MATLAB implementation of the proposed gradient based vessel detection algorithm tested on DRIVE database image requires approximately 1.83 s second to process.

Table 2.8 shows that the proposed gradient based search method requires in average a time of only 1.83 s which is slightly higher than only one method so far available in literature [14] but it provides comparatively higher accuracy. Moreover, [14] employs vessel segmentation by thresholding wavelet coefficients. But in this thesis, it is observed that spectral domain does not provide satisfactory performance for vessel segmentation.

Table 2.6: Performance metrics obtained by using the proposed method on STARE database images with adaptive median filtering and  $N_p = 3$

Image	$Se$	$Sp$	$Ppv$	$Npv$	$Acc$ in percentage
1	0.7425	0.9399	0.6011	0.9677	91.8453
2	0.6754	0.9645	0.6692	0.9655	93.6723
3	0.8682	0.8649	0.3656	0.9865	86.5202
4	0.4504	0.9881	0.8158	0.9390	93.1914
5	0.8546	0.8887	0.5229	0.9772	88.4414
6	0.9122	0.9051	0.4843	0.9906	90.5764
7	0.8888	0.8998	0.5231	0.9850	89.8557
8	0.9004	0.9188	0.5602	0.9877	91.6870
9	0.8792	0.9227	0.5790	0.9844	91.8011
10	0.8704	0.8803	0.4753	0.9820	87.9189
11	0.8966	0.9274	0.5755	0.9879	92.4316
12	0.9526	0.9178	0.5811	0.9939	92.1542
13	0.8566	0.9324	0.6389	0.9790	92.3129
14	0.8566	0.9295	0.6356	0.9783	92.0353
15	0.8105	0.9484	0.6791	0.9738	93.1985
16	0.6878	0.9650	0.7656	0.9489	92.5442
17	0.8534	0.9497	0.7058	0.9786	93.7766
18	0.6698	0.9892	0.8251	0.9752	96.6638
19	0.6658	0.9813	0.6886	0.9793	96.2894
20	0.7362	0.9496	0.5988	0.9724	92.9787
<i>Avg</i>	0.8014	0.9332	0.6145	0.9766	91.9945

Table 2.7: Performance Metrics Compared To Other Methods On The Stare And Drive Databases In Terms Of Average Accuracy

Method Type	Method	DRIVE	STARE	DRIVE+ STARE
<b>Ruled-Based</b>	Chaudhuri <i>et al.</i> [7]	0.8773	–	–
	Hoover <i>et al.</i> [23]	–	0.9275	–
	Jiang and Mojon [9]	0.8911	0.9009	0.8960
	Mendonça <i>et al.</i> [6]	0.9463	0.9479	0.9471
	Martinez-Perez <i>et al.</i> [12]	0.9344	0.9410	0.9377
	Cinsdikici and Aydin [8]	0.9293	–	–
	Proposed Method	0.9390	0.9391	0.939

## 2.6 Conclusion

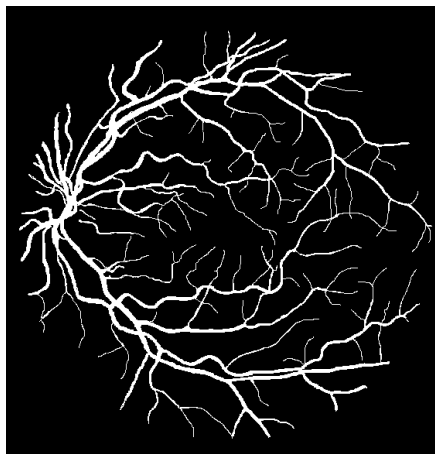
In this chapter, first, some vessel enhancement schemes are proposed, which are essential prior to vessel pixel detection. It is found that in order to reduce noises

Table 2.8: Time requirements by different vessel detection algorithms. Here, Impl=Implementation, M=MATLAB

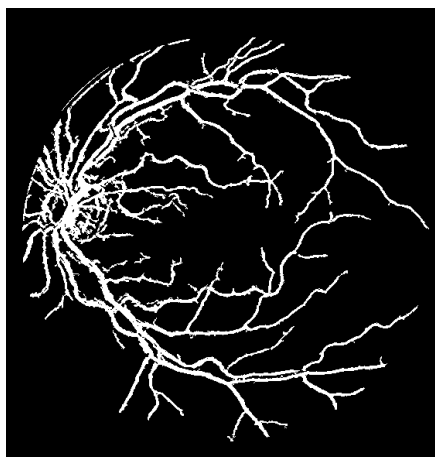
<b>Method</b>	<b>Processor</b>	<b>RAM</b>	<b>Impl</b>	<b>Accuracy</b>	<b>Time</b>
Bankhead [14]	2.13 GHz	2 GB	M	0.9371	0.093 s
Espona [11]	1.83 GHz	2 GB	C++	0.9352	38.4 s
Mendonca [6]	3.2 GHz	960 MB	M	0.9463	< 150 s
Proposed(Search)	2.5 GHz	2 GB	M	0.9390	1.830 s
Proposed(Classification)	2.5 GHz	2 GB	M	0.9423	13.114 s

from the retinal images, adaptive median filtering technique offers better performance in comparison to the repeated median filtering technique. It is shown that, along with any one of these vessel enhancement techniques, if morphological opening operation can be utilized by employing the Top-Hat transform, a significantly improvement in the enhancement performance can be obtained. Next, an intensity gradient based bidirectional search scheme is proposed to extract vessel pixels from enhanced retinal images. In the search scheme, the effect of variation of the number of pixels considered within neighborhood on detection accuracy is also investigated. Finally some morphological operation based post-processing schemes are utilized to reduce the false vessel detection. Vessel detection performance is evaluated on two publicly available standard retinal image databases and it is observed that the proposed scheme provides satisfactory performance in comparison to some of the existing methods both in terms of vessel detection accuracy as well as computational complexity.

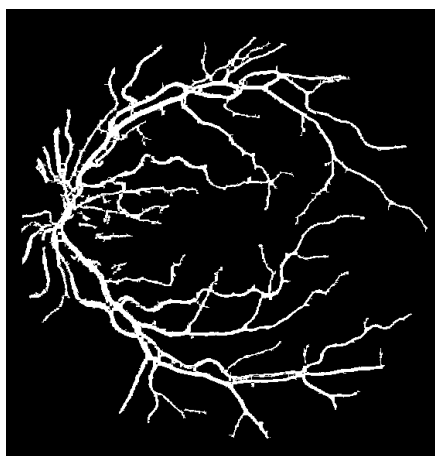




(a)



(b)



(c)

Fig. 2.5: Comparison among output binary images obtained by using the proposed method: (a) ground truth values obtained using the manual labeling by expert, which is available in database, (b) proposed gradient based vessel segmentation with repetitive median filtering, and (c) adaptive median filtering.

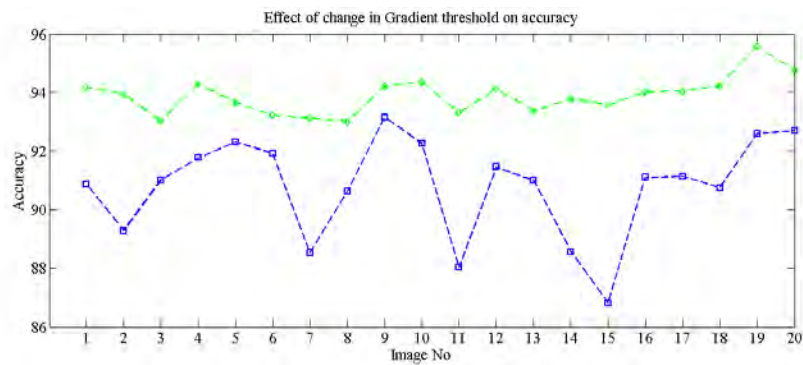


Fig. 2.6: Accuracy plot of Comparison between Gradient Threshold 3 and 5 on DRIVE database. Blue and Green color represent accuracy for Threshold 3 and 5 respectively.

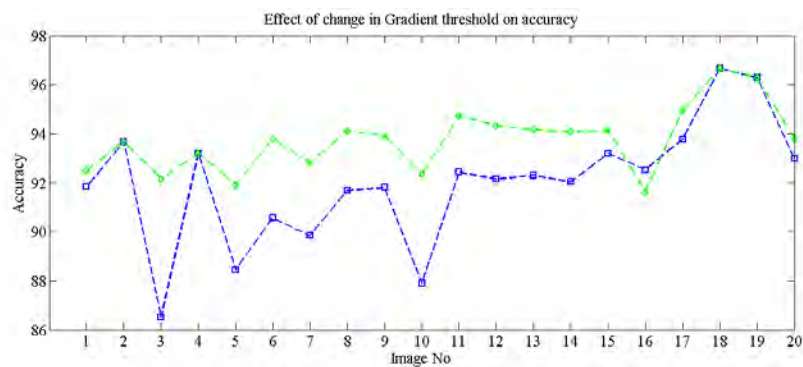
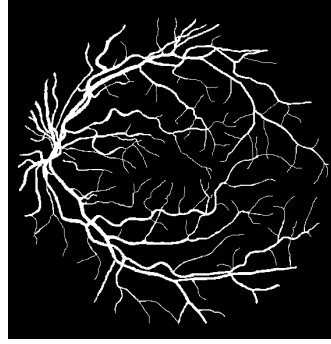
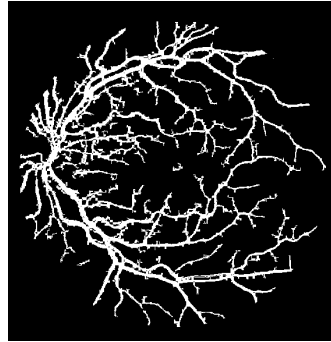


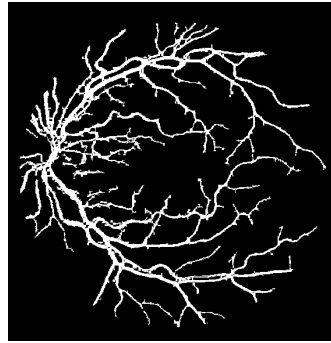
Fig. 2.7: Accuracy plot of Comparison between Gradient Threshold 3 and 5 on STARE database images. Blue and Green color represent accuracy for Threshold 3 and 5 respectively.



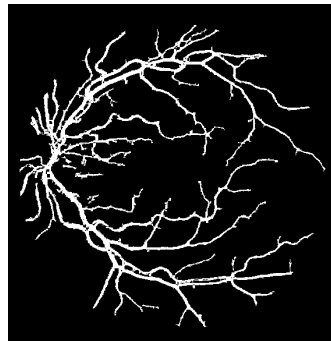
(a)



(b)

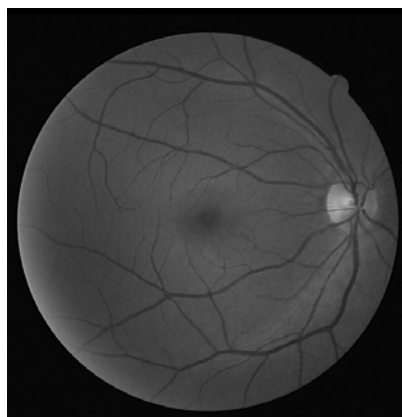


(c)

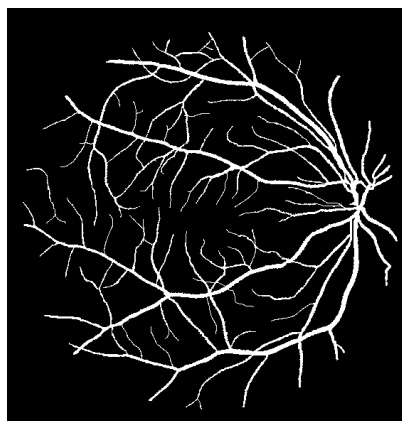


(d)

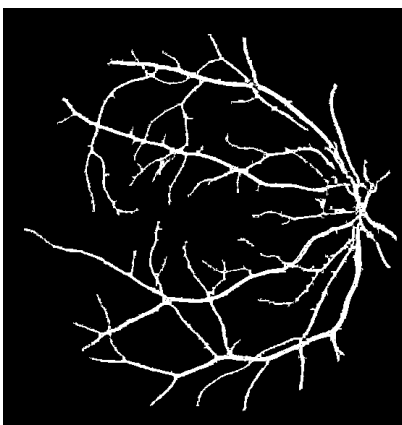
Fig. 2.8: Comparison among output binary images obtained by using the proposed gradient based search method with different values of neighboring pixel  $N_p$ . (a) Manual labeling available in the database, and vessel detection outcome with proposed gradient based threshold for (b)  $N_p = 3$ , (c)  $N_p = 4$ , and (d)  $N_p = 5$ .



(a)

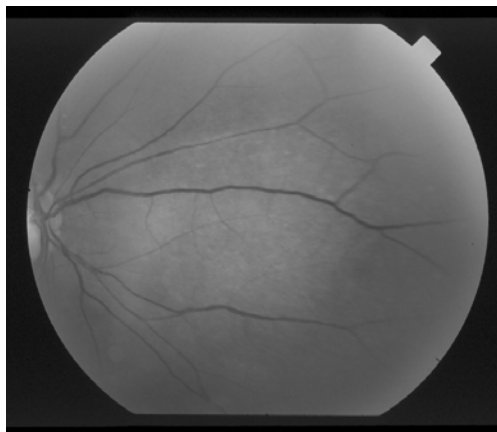


(b)

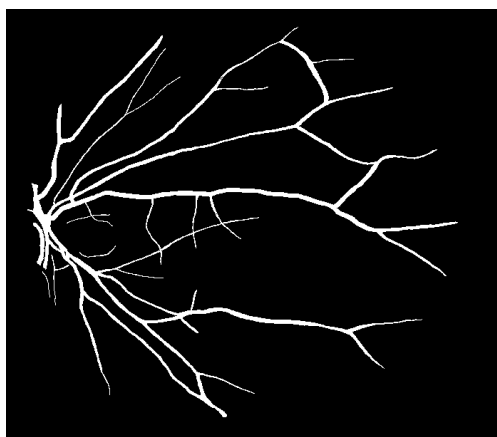


(c)

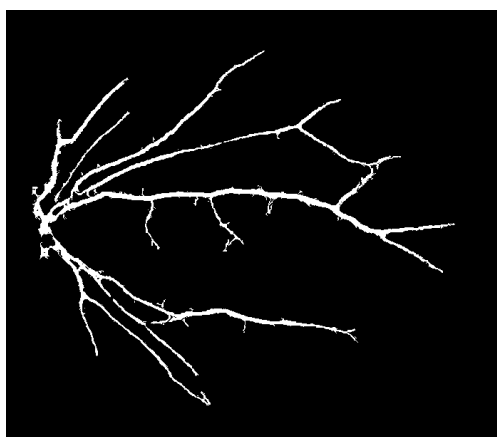
Fig. 2.9: Illustration of the spatial location of classification errors on a DRIVE image. (a) Green plane image, (b) ground truth blood vessels, and (c) detected blood vessels using the proposed method.



(a)



(b)



(c)

Fig. 2.10: Illustration of the spatial location of classification errors on a STARE image. (a) Green plane image, (b) ground truth blood vessels, and (c) detected blood vessels using the proposed method.

# Chapter 3

## Proposed Vessel Pixel Classification Scheme

The problem of retinal vessel detection can be formulated as pixel by pixel classification of the retinal image into two classes, vessel and non-vessel. In that case, for the purpose of classification, it would be a challenging task to obtain consistent features from just a given pixel. Moreover, depending on the resolution of the retinal image, pixel by pixel classification will involve huge computational burden. In this chapter, an efficient scheme for retinal vessel pixel classification is proposed with two fold objectives: (1) to extract better vessel pixel characteristics for obtaining high classification accuracy and (2) to overcome the computational burden generally involved in classification based methods. It is to be mentioned that pixel feature extraction strongly depends on vessel pixel enhancement. Unlike the gradient search based vessel detection, pixel feature extraction involves a neighboring zone centered at the test pixel, which calls for effective vessel image enhancement technique. During vessel feature extraction from an enhanced image, we propose to utilize shifted spatial zones apart from the central spatial zone. Moreover both spatial and spectral features are taken into consideration. On the other hand to reduce the computational burden, instead of dealing with all pixels of a retinal image, only some primarily selected candidate vessel pixels are considered for classification. The gradient search based vessel detection method proposed in the last chapter is used to obtain vessel candidate pixels. It is obvious that a significant portion of the candidate pixels, although detected as vessel in gradient search based method, may not be actually vessel. That is some non-vessel pixels situated outside the vessel edge generally get included as vessel pixel in the vessel detection process. In order to overcome this error and reduce the number of ‘False Positive’, these vessel candidates are then

classified extracting suitable features and employing a suitable classifier. In order to obtain better accuracy by using the classifier, one very important aspect is the development of efficient trainer. To the best of our knowledge, all the retinal pixel classification methods reported so far rely on manual selection of training pixels. As a result, the accuracy of pixel classification in testing phase strongly depends on selected training data. Another objective in this chapter is to develop a scheme for universal training pixel selection, which will overcome the dependency on manual selection or eye inspection. Pixels declared to be non-vessel by the classifier are excluded from the binary image obtained in candidate selection process. The resultant image is compared with the ground truth provided in the database and accuracy of the whole method, combining candidate selection and classification, is determined. Therefore, the next method of vessel pixel classification consists of the following steps:

1. Preprocessing of green plane image
2. Feature Extraction
3. Train formation or trainer pixel selection
4. Classification

### **3.1 Preprocessing**

As discussed in the previous chapter that the preprocessing step is extremely important to reduce the effect of lighting variations, poor contrast and noise. Thus, it is obvious that for efficient feature extraction required by the classification procedure rely on the quality of preprocessing. It is found in the previous chapter that the preprocessing technique based on adaptive median filtering or repeated median filtering can provide better intensity variation among the vessel and non-vessel pixels located on a row (or column) of a retinal image. However, in pixel feature extraction it is necessary to consider a region centered at the test pixel. In this case, the effect of background intensity variation due to nonuniform illumination may worsen the performance of the vessel segmentation methodology.

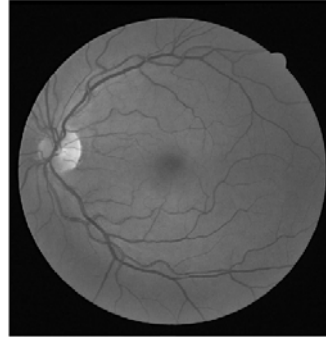
### 3.1.1 Background Homogenization based on Shade Correction

As discussed in the previous chapter, fundus photos often contain an intensity variation in the background across the image, called “vignetting”. Vignetting is the result of an improper focusing of light through an optical system. The result is that the brightness of the image generally decreases radially outward from near the center of the image. A retinal image is captured by viewing the inner rear surface of the eyeball through the pupil. The lens of the camera works in conjunction with the lens of the eyeball to form the image. Since the position of the eye relative to the camera varies from image to image, the exact properties of the vignetting also vary from image to image. With the purpose of removing these background lighting variations, a preprocessing method suitable for feature extraction is devised in this chapter. In this method, a shade-corrected image is accomplished from a background estimate. This image is the result of a filtering operation with a large arithmetic mean kernel, as described below.

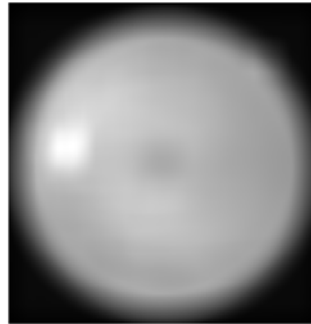
Firstly, a background image,  $I_B$  is produced by convolving the green plane image,  $I_G$  with a mean kernel of dimensions  $m \times m = 69 \times 69$ . Then, the difference, known as shade corrected image,  $I_{SC}$ , between main green plane image and background image is calculated for every pixel. To this respect, literature reports shade-correction methods based on the subtraction of the background image from the original image in [1], [2] and [30], or the division of the latter by the former in [31]. Both procedures rendered similar results upon testing. Moreover, none of them showed to contribute any appreciable advantage relative to the other. The subtractive approach was used in the present work.

In Fig. 3.1, an image from DRIVE database has been represented with its green plane image, nature of the background image formed and resultant shade corrected image. It is clearly observed that due to shade correction, all the FOV pixels or in other words, the blood vessel pixels could be brought on the same plane or homogenized background.

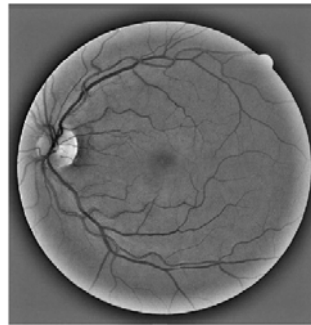




(a)



(b)



(c)

Fig. 3.1: Shade Corrected Image Formation. (a) Green Plane Image. (b) Background Image. (c) Shade Corrected Image.

### 3.1.2 Vessel Enhancement by Sequential Opening Filtering and Top-Hat Transform

Next in view of obtaining further enhancement of vessel pixels in shade corrected image  $I_{SC}$ , in the proposed scheme, Top-Hat transform based morphological operation is carried out. Subtracting an opened image (i.e. an image being processed using morphological opening operation) from the original image is called Top-Hat Transform. It is well known that the morphological opening operation can remove completely regions of an object, which cannot contain the structuring element, smooth

object contours, breaks, thin connections, and can remove thin protrusions. In Fig. 3.2, effect of opening and closing operation is presented. In the proposed scheme, for visual convenience, the Top-Hat transform operation is performed on the complementary image of  $I_{SC}$ , i.e., the vessel enhanced image  $I_{VE}$  can be expressed as

$$I_{VE} = I_{SC}^C - \gamma(I_{SC}^C) \quad (3.1)$$

where  $\gamma$  is a morphological opening operation using a disc of suitable size. Thus, while bright retinal structures are removed (i.e., optic disc, possible presence of exudates or reflection artifacts), the darker structures remaining after the opening operation become enhanced (i.e., blood vessels, fovea, possible presence of microaneurysms or hemorrhages).

### Morphological Opening Operation

The operations of dilation and erosion are fundamental image processing. Dilation is an operation that grows or thickens objects in an image. The specific manner and extent of this thickening is controlled by a shape referred to as structuring element. The dilation of A by B denoted as  $A \oplus B$ , is defined as the set operation,

$$A \oplus B = z | (\hat{B}_z) \cap A \neq \phi \quad (3.2)$$

Erosion shrinks or thins objects in a binary image. As in dilation, the manner of extent of shrinking is controlled by a structuring element. The erosion of A by B denoted as  $A \ominus B$ , is defined as the set operation,

$$A \ominus B = z | (B_z) \subseteq A \quad (3.3)$$

The morphological opening operation of A by B denoted  $A \circ B$ , is defined as the erosion of A by B, followed by a dilation of the result by B. An equivalent formulation of opening is

$$A \circ B = \cup(B)_z | (B)_z \subseteq A \quad (3.4)$$

where  $\cup \cdot$  denotes the union of all sets inside the braces.

It is to be mentioned that the opening operation suppresses bright details of an object smaller than the structuring element [29]. One may use sequential opening operation with a series of structuring elements of increasing size is carried out. In

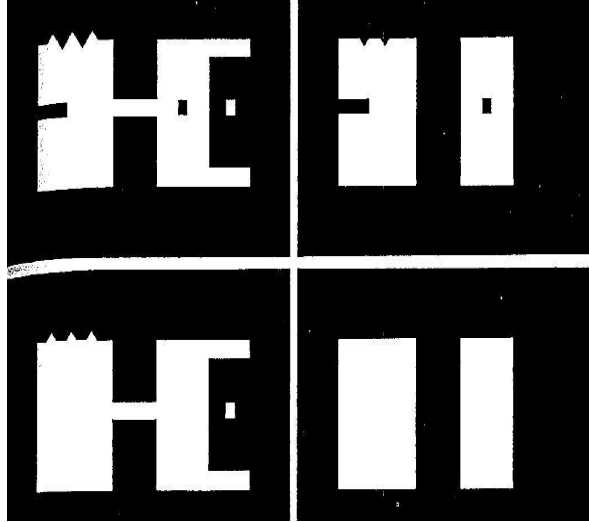


Fig. 3.2: Top Left: Original image, Top Right: Opening, Bottom Left: Closing, Bottom Right: Closing of Bottom Left Figure

case of shade corrected image, we propose to employ the Top-Hat transformation on repeatedly opened image  $I_{SC}^C$ . Number of repetition depends on the amount of increase in the disc radius used for the opening operation. Here the repetition is performed for seven times as at each stage of morphological opening operation the disc radius is increased by a very small amount, only single pixel starting from one pixel.

In the proposed method in this chapter, vessel enhancement is performed by estimating the complementary image of the shade corrected image,  $I_{SC}^C$  and subsequently applying the morphological Top-Hat transformation on consequently seven times morphologically opened image  $I_{SC}^C$ . At each stage of morphological opening operation, the disc radius is increased by one pixel starting from one pixel. All the features are then extracted from this final step preprocessed vessel enhanced image  $I_{VE}$ .

Fig. 3.3 shows the sequential steps of the vessel enhancement operation on the shade corrected image and the resultant enhanced image which evidently demonstrates the lucid appearance of the blood vessels with respect to the background.

The effect of vessel enhancement in these figures may not be visible by eye inspection. In the result section of this chapter, results obtained from images preprocessed in both methods are shown and their efficiencies are compared, which clearly demon-

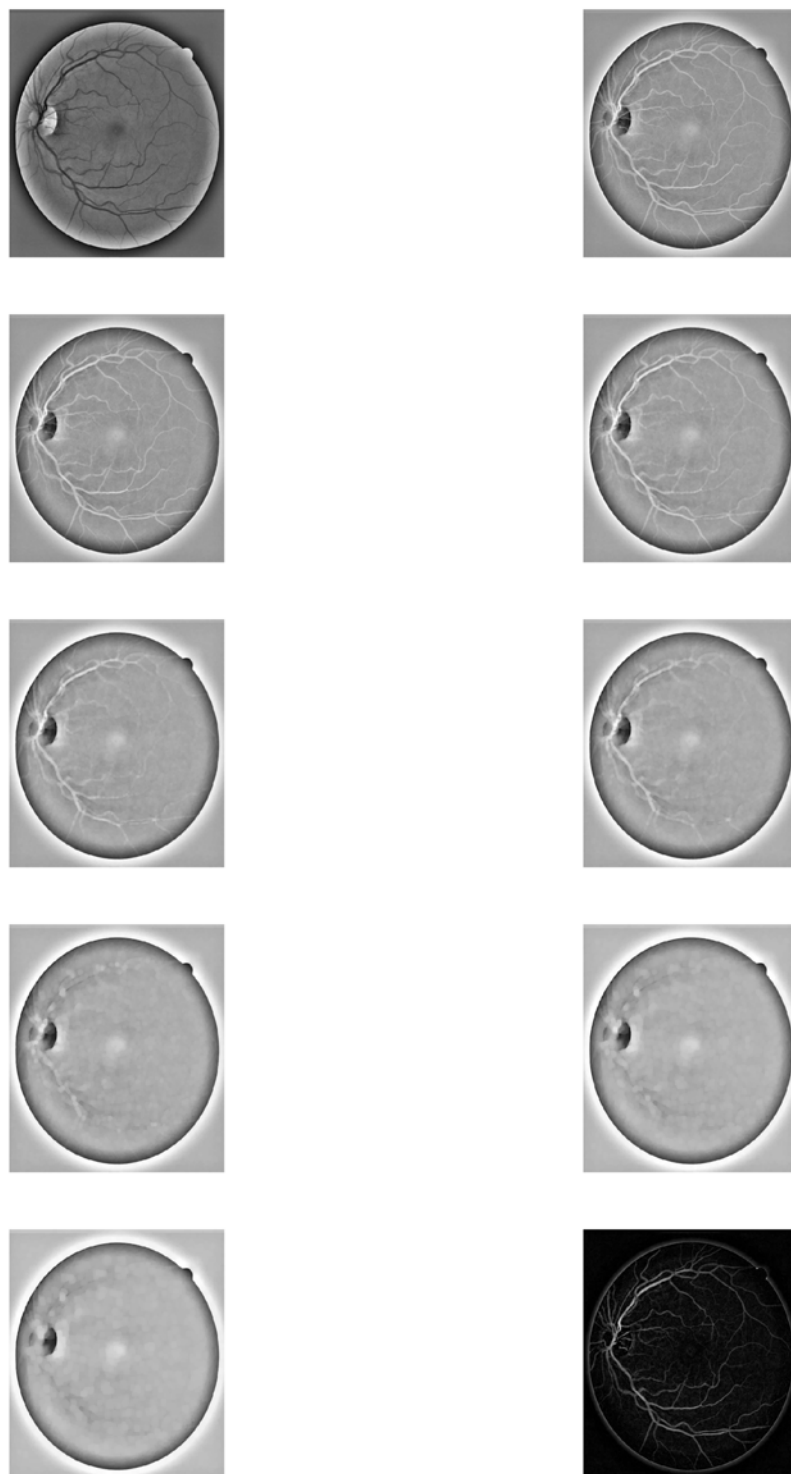


Fig. 3.3: Sequential Opening Filtering before Top-Hat Transform. Top Left: Shade Corrected Image. Top Right: Complementary Image. Following Images: Sequential Opening Filtering. Bottom Right: Top-Hat Transformed Image

strate the advantage of using the adaptive median filtering based method and the reasons behind have already explained.

## 3.2 Feature Extraction

The major objective of the feature extraction stage is pixel characterization by means of a feature vector, a pixel representation in terms of some quantifiable measurements which may be easily used in the classification stage to decide whether pixels belong to a real blood vessel or not. In gradient based search method for vessel candidate selection discussed in the previous chapter, only neighboring pixels of the test pixel, which are located on the same row (or column) where the test pixel is located, are considered to determine the nature of the pixel. However, in this chapter, a subregion (or a block) around a test pixel is taken into account and features are extracted from that subregion (or block). It is expected that the local block based feature extraction would help in better determination of vessel candidacy. In the proposed method, the following sets of features are selected:

- **Spatial intensity based features:** These features are computed based on the spatial intensity variation of the local block corresponding to the candidate pixel.
- **Spectral features:** These features are computed based on the spectral variation of the local block corresponding to the candidate pixel.

### 3.2.1 Spatial intensity based features

Spatial intensity based features can be divided into two following categories:

- **Spatial statistical features**
- **Shifted spatial statistical features**

Since blood vessels are always darker than their surroundings, features based on describing intensity-level variation in the surroundings of candidate pixels seem to be a good choice. Some widely used statistical measures suitable for capturing spatial intensity variation are chosen to extract features from preprocessed green plane image [21]. Here, only a small surrounding region centered on the candidate pixel  $I_{VE}(x, y)$  will be considered for feature extraction. Denoting  $S_{x,y}^\omega$  to represent a set of coordinates in a  $\omega \times \omega$  sized square spatial block centered on the point  $(x, y)$ , five spatial statistical features can be expressed as shown in Table 3.1.

Table 3.1: Definition of some spatial features in Mathematical terms

Title	Equation
<b>Distance from Block Minima</b>	$f_1(x, y) = I_{VE}(x, y) - \min_{(s,t) \in S_{x,y}^\omega} I_{VE}(s, t)$
<b>Distance from Block Maxima</b>	$f_2(x, y) = \max_{(s,t) \in S_{x,y}^\omega} I_{VE}(s, t) - I_{VE}(x, y)$
<b>Distance from Block Average</b>	$f_3(x, y) = I_{VE}(x, y) - \text{mean}_{(s,t) \in S_{x,y}^\omega} I_{VE}(s, t)$
<b>Standard Deviation of Block</b>	$f_4(x, y) = \text{std}_{(s,t) \in S_{x,y}^\omega} I_{VE}(s, t)$
<b>Candidate Pixel Value</b>	$f_5(x, y) = I_{VE}(x, y)$

Motivation behind choosing these particular spatial features is their conventional statistical behavior, which is expected to provide clear separation between spatial characteristics of two types of pixels, vessel and non-vessel. A histogram based analysis is carried on to justify the quality of these statistical features. Detailed description of each of these features is given as follows.

### Distance from Block Minima

The feature  $f_1(x, y)$ , described in Table 3.1, extracts the difference between the intensity value of the candidate pixel  $I_{VE}(x, y)$  and minimum intensity value of the block  $S_{x,y}^\omega$  around it. In the preprocessed green plane of a retinal image, vessel pixels are brighter than the nonvessel ones. If a subregion centered on a vessel pixel contains both vessel and nonvessel pixels, obviously one of the nonvessel pixels will contain minimum intensity. Hence, in order to be a vessel pixel, the center pixel must have an intensity higher than that particular minimum pixel intensity. That is, this particular feature must attain a high value for any vessel pixel situated along the edge of a vessel with the probability of having nonvessel pixels around it. Histogram of this feature value computed for equal number of randomly chosen vessel and non-vessel pixels of a retinal image taken from the DRIVE database is shown in Fig. 3.4. Here we consider a total of 40,000 pixels and a block size of  $5 \times 5$ . As expected, the feature values for non-vessel pixels are found very small in almost all cases. This histogram shows a clear distinction between the characteristics of vessel and non-vessel pixels based on this feature. Hence, it is expected that this particular feature can even handle the critical case, that is differentiating the pixels situated at the vessel edge and just outside the edge.

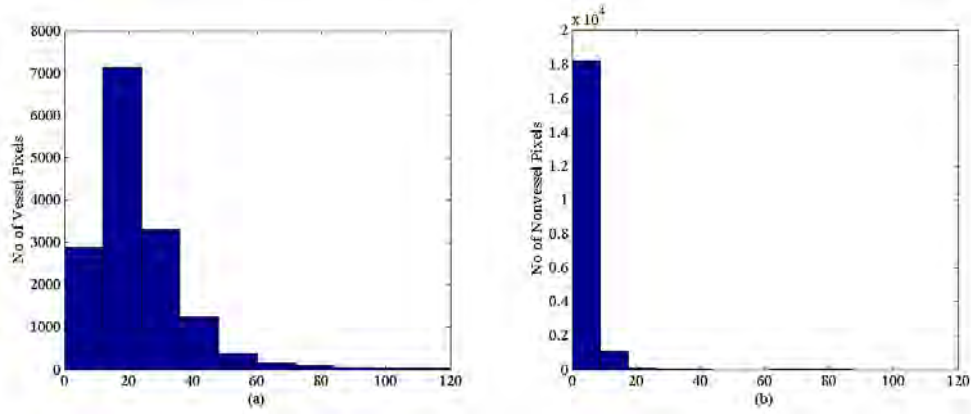


Fig. 3.4: Histogram computed for vessel pixels (left figure) and non-vessel pixels (right figure) corresponding to the first spatial statistical feature ( $f_1$ ): difference between the intensity value of the central pixel  $I_{VE}(x, y)$  and minimum intensity value of the block  $S_{x,y}^\omega$ .

### Distance from Block Maxima

The feature  $f_2(x, y)$ , described in Table 3.1, extracts the difference between the intensity value of the candidate pixel  $I_{VE}(x, y)$  and maximum intensity value of the block  $S_{x,y}^\omega$ . If a subregion centered on a vessel pixel contains both vessel and nonvessel pixels, obviously one of the vessel pixels will contain minimum intensity. Hence, in order to be a vessel pixel, the center pixel must have an intensity value very close to that particular minimum pixel intensity. That is, this particular feature must attain a low value for any pixel situated along the edge of a vessel or along the midline of a vessel. In a similar fashion as shown in Fig. 3.4, the histogram of this feature value computed for equal number of randomly chosen vessel and non-vessel pixels of a retinal image is shown in Fig. 3.5. As expected, the feature values for vessel pixels are found small in most of the cases. Unlike the histogram obtained for the first feature, this histogram shows some overlap in the feature value, which indicates that the classification performance of the previous feature is expected to be better than this feature. However, it is clearly observed that it has some differences in case of a number of pixels, which may help in classification.

### Distance from Block Average

The feature  $f_3(x, y)$ , described in Table 3.1, extracts the difference between the intensity value of the candidate pixel  $I_{VE}(x, y)$  and average intensity of the pixels

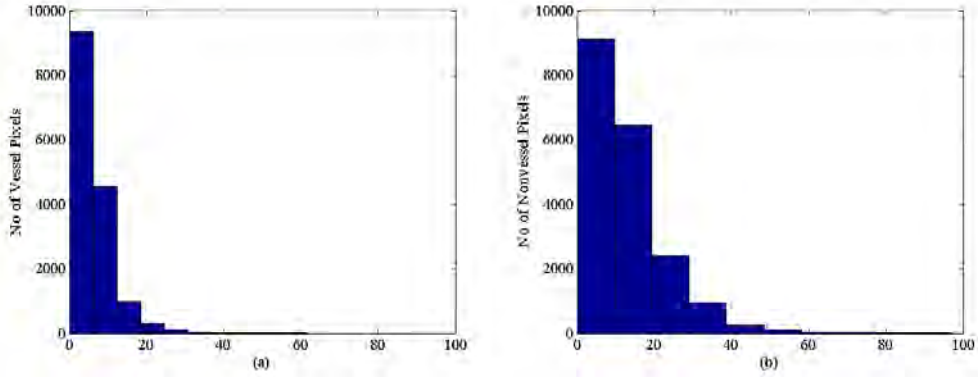


Fig. 3.5: Histogram computed for vessel pixels (left figure) and non-vessel pixels (right figure) corresponding to the second spatial statistical feature ( $f_2$ ): difference between the intensity value of the central pixel  $I_{VE}(x, y)$  and maximum intensity value of the block  $S_{x,y}^\omega$ .

lying inside the block  $S_{x,y}^\omega$ . A vessel pixel is generally surrounded by some other vessel pixels when a small block is considered. This fact is also true for the non-vessel pixels. Since the intensity value of a candidate vessel pixel is generally very high in comparison to the non-vessel pixels, this particular feature value will be positive as well as high for vessel pixels, while the feature value will be lower or mostly negative for non-vessel pixels. This is clearly visible in the histogram plots shown in Fig. 3.6. This histogram plots demonstrate better distinguishable characteristics of vessel and non-vessel pixels based on this feature. Thus, it is expected to differentiate well between any pixel located inside or outside a vessel.

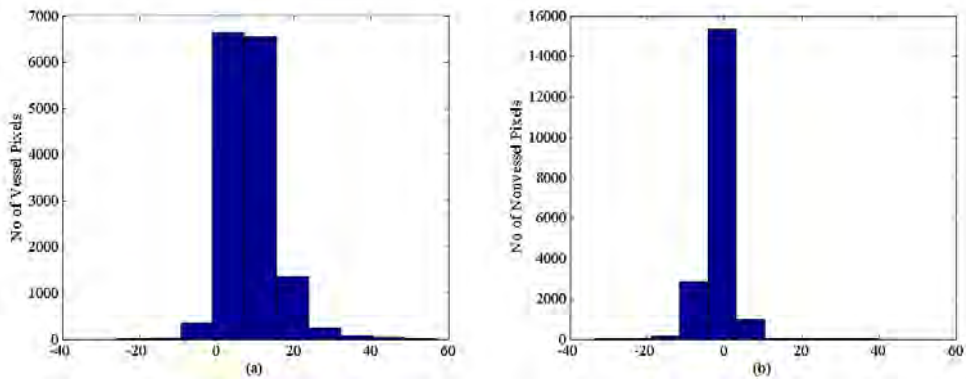


Fig. 3.6: Histogram computed for vessel pixels (left figure) and non-vessel pixels (right figure) corresponding to the third spatial statistical feature ( $f_3$ ): difference between the intensity value of the central pixel  $I_{VE}(x, y)$  and average intensity of the block  $S_{x,y}^\omega$ .



### Standard Deviation of Block

The feature  $f_4(x, y)$ , described in Table 3.1, extracts the standard deviation of the pixels lying inside the block  $S_{x,y}^\omega$ . It is well known that the vessel pixel values are comparatively much higher than those of the non-vessel pixels. It is found that the standard deviation of pixel intensities inside a vessel is usually higher than that obtained outside the vessel. Hence, it is expected that the center pixel, if it is a vessel pixel, generally belong to a block with high standard deviation. That is, this particular feature will exhibit a high value for a candidate vessel pixel. This fact is also visible in the histogram plots shown in Fig. 3.7. The histogram plots demonstrate a clear distinction between the characteristics of vessel and non-vessel pixels based on this feature, which leads to an expectation of better pixel classification both inside and outside a vessel.

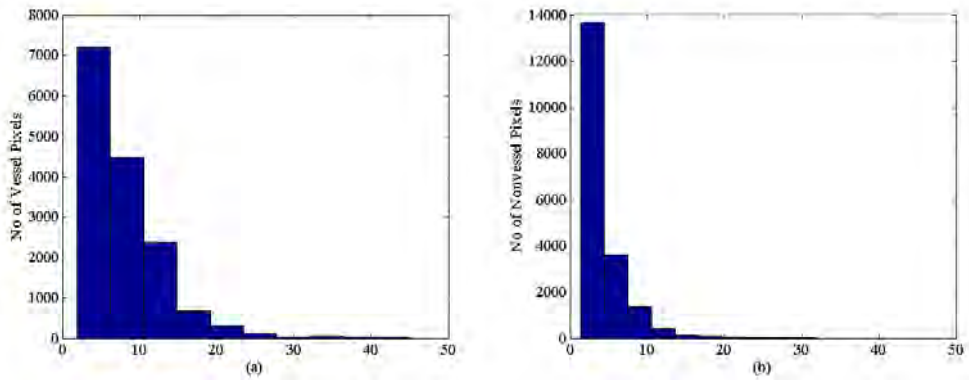


Fig. 3.7: Histogram computed for vessel pixels (left figure) and non-vessel pixels (right figure) corresponding to the fourth spatial statistical feature ( $f_4$ ): standard deviation of the pixel intensities of a block  $S_{x,y}^\omega$ .

### Candidate Pixel Value

The feature  $f_5(x, y)$ , described in Table 3.1, refers to intensity value of the pixel under consideration. As stated earlier, in the preprocessed green plane of a retinal image, the vessel pixel values are comparatively much higher than those of the non-vessel pixels. This particular feature must attain a high value for any pixel situated along the edge of a vessel (weak vessel pixels) or along the midline of a vessel (strong vessel pixels). Histogram plots of this feature are shown in the Fig. 3.8. The histogram plots show a clear distinction between the characteristics of

vessel and non-vessel pixels based on this feature. Hence, it is expected that this particular feature can efficiently differentiate the pixels situated both inside and outside a vessel.

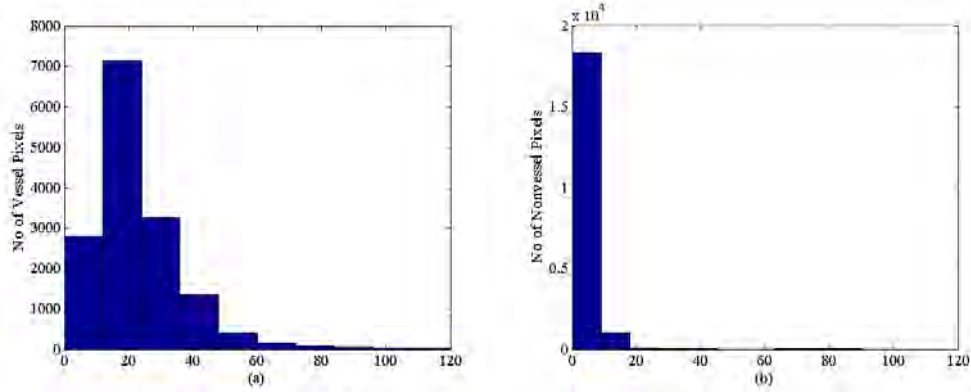


Fig. 3.8: Histogram computed for vessel pixels (left figure) and non-vessel pixels (right figure) corresponding to the fifth spatial statistical feature ( $f_5$ ): intensity of the candidate pixel.

### Shifted Spatial Feature

All spatial statistical features are computed from a small block centered at the candidate pixel. That is each pixel corresponds to a set of features obtained from a block. However, it is more likely that a vessel candidate pixel is generally surrounded by some other vessel pixels. Similarly, a non-vessel pixel is generally surrounded by some other non-vessel pixels. In order to utilize such a natural phenomenon, it is more logical that prior to take decision about a candidate pixel, instead of relying only on a single block that corresponds to it, some neighboring blocks corresponding to the neighborhood pixels should also be taken in to consideration. Hence in the proposed method, for a central  $n \times n$  block,  $(n^2 - 1)$  number of neighboring blocks corresponding to the  $(n^2 - 1)$  neighborhood pixels are considered for feature extraction. In fact, the neighboring blocks will carry information related to spatially shifted region. Each of those five spatial statistical features will be computed for each spatially shifted block. For example, for a  $3 \times 3$  central block, there will be 8 spatially shifted blocks. The main concern is to investigate the feature consistency in each block. Thus, it is sufficient to consider only the mean and median of block features,

i.e., in the above example, considering the mean and median of eight features. In Fig. 3.9, the location of shifted blocks from the central block corresponding to the candidate pixel is shown. Instead of taking all eight set of features, mean and median of each feature computed from all sets are considered as features. Mean and median of the block features can provide an overall idea of the neighborhood condition of the center pixel and help to determine the class of the candidate pixel. It is expected that these additional spatially shifted statistical features in combination with the spatial statistical features can provide better feature quality. Similar to the case of spatial statistical features, the quality of the extracted spatial shifted features is shown with the help of histograms in Fig. 3.10, Fig. 3.11, Fig. 3.12, Fig. 3.13 and Fig. 3.14. Here a  $3 \times 3$  central block and 8 spatially shifted blocks are considered for the same image as shown in 3.4. In these figures, for each feature, mean and median feature values are plotted. It is clearly observed that the histograms show well separation between characteristics of vessel and non-vessel pixels.

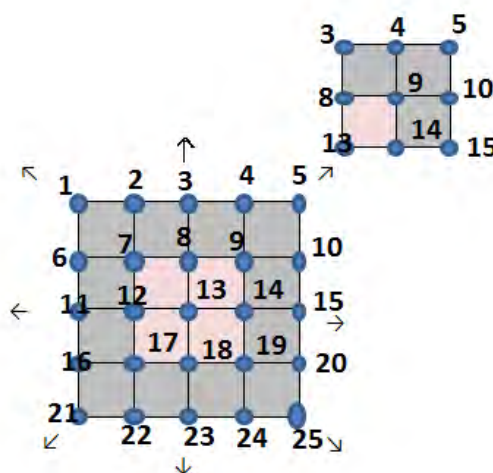


Fig. 3.9: Location of blocks on which spatially shifted features are computed. Here, 13 no pixel and pink colored block represent pixel to be tested and the block around it respectively. Isolated block depicts the position of center pixel of each shifted block with respect to the test pixel.

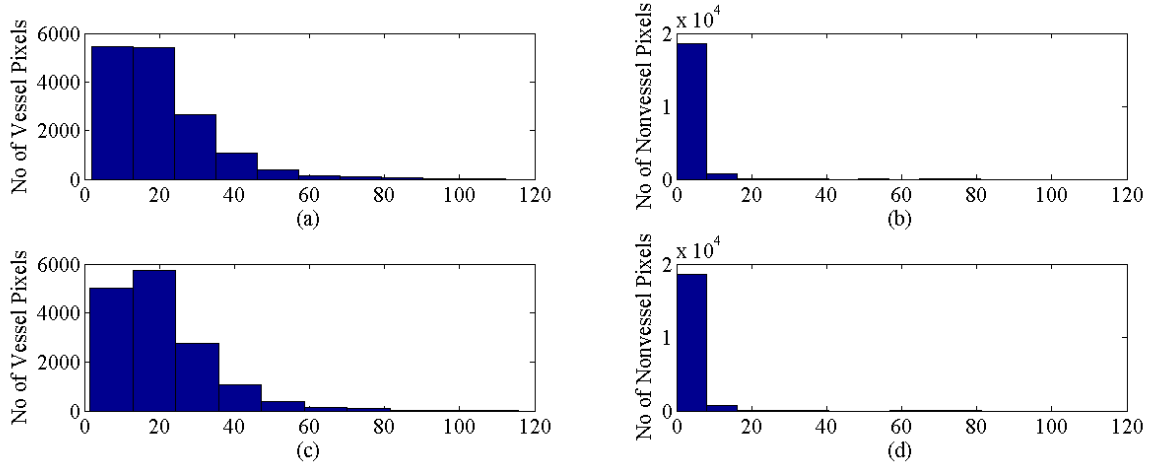


Fig. 3.10: Histograms computed for vessel pixels (left figure) and non-vessel pixels (right figure) of all shifted blocks. Mean (top figure) and median (bottom figure) of spatially shifted feature values corresponding to the first feature ( $f_1$ ).

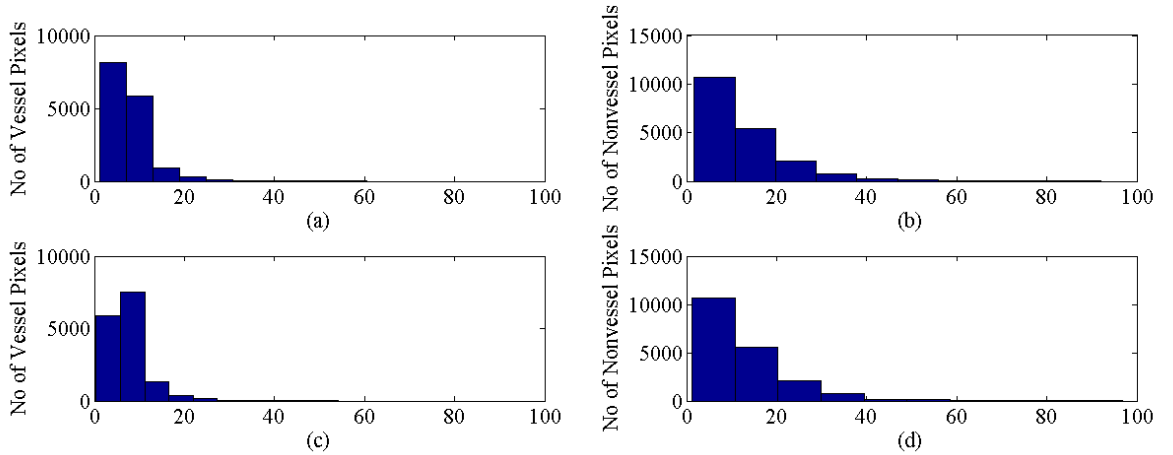


Fig. 3.11: Histograms computed for vessel pixels (left figure) and non-vessel pixels (right figure) of all shifted blocks. Mean (top figure) and median (bottom figure) of spatially shifted feature values corresponding to the second feature ( $f_2$ ).

### 3.2.2 Spectral Features

Apart from the spatial features, in the proposed method, spectral characteristics of the spatial blocks are also proposed to be used as competitive feature for retinal pixel classification. A frequency domain feature extraction algorithm using two dimensional discrete cosine transform (2D-DCT) is developed, which operates within the small blocks to extract dominant spectral features. It is to be mentioned that Fourier transform based feature extraction algorithms involve complex computations. In contrast, DCT of real data avoids complex arithmetic and offers ease of implementation in practical applications. Moreover, DCT can efficiently handle the

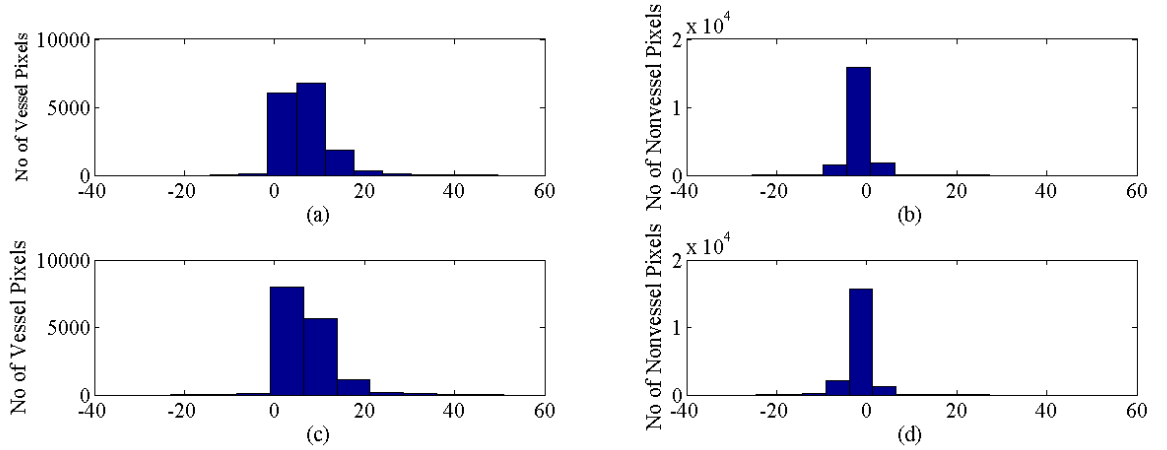


Fig. 3.12: Histograms computed for vessel pixels (left figure) and non-vessel pixels (right figure) of all shifted blocks. Mean (top figure) and median (bottom figure) of spatially shifted feature values corresponding to the third feature ( $f_3$ ).

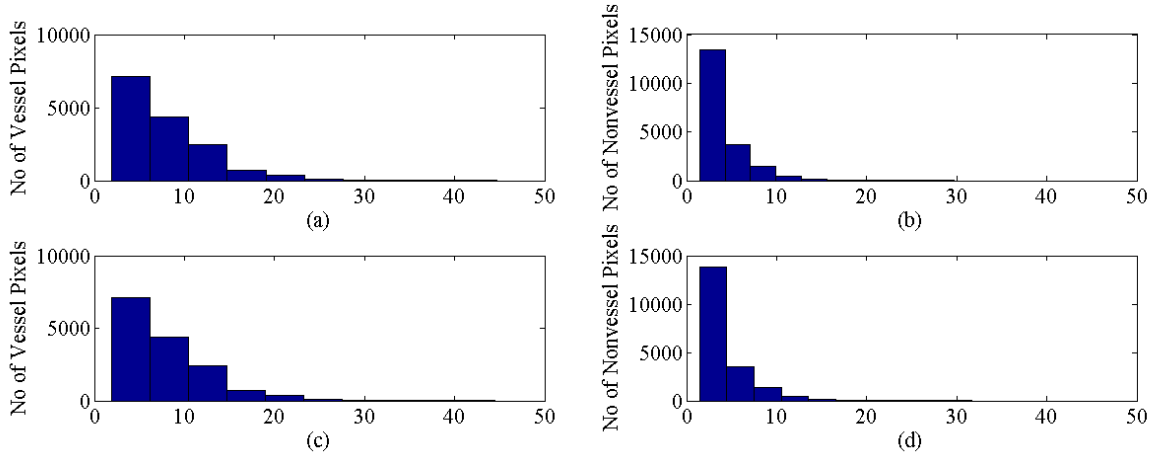


Fig. 3.13: Histograms computed for vessel pixels (left figure) and non-vessel pixels (right figure) of all shifted blocks. Mean (top figure) and median (bottom figure) of spatially shifted feature values corresponding to the fourth feature ( $f_4$ ).

phase unwrapping problem and exhibits a strong energy compaction property, i.e., most of the signal information tends to be concentrated in a few low-frequency components of the DCT. Hence, we intend to develop an efficient feature extraction scheme using 2D-DCT.

For a function  $f(x, y)$  with dimension of  $M \times N$ , the 2D-DCT  $F(p, q)$  also has dimension  $M \times N$  and is computed as

$$F(p, q) = \alpha_p \alpha_q \sum_{x=0}^{M-1} \sum_{y=0}^{N-1} f(x, y) \cos \frac{\pi(2x+1)p}{2M} \cos \frac{\pi(2y+1)q}{2N} \quad (3.5)$$

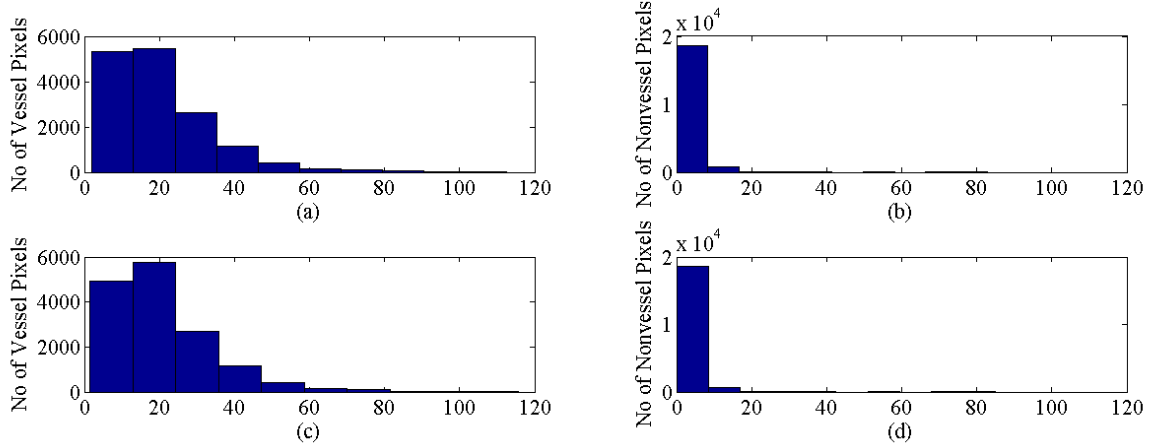


Fig. 3.14: Histograms computed for vessel pixels (left figure) and non-vessel pixels (right figure) of all shifted blocks. Mean (top figure) and median (bottom figure) of spatially shifted feature values corresponding to the fifth feature ( $f_5$ ).

Here  $0 \leq p \leq M - 1$ ,  $0 \leq q \leq N - 1$  and

$$\alpha_p = \begin{cases} \frac{1}{\sqrt{M}}, & \text{if } p = 0. \\ \sqrt{\frac{2}{M}}, & \text{if } 1 \leq p \leq M - 1. \end{cases} \quad (3.6)$$

$$\alpha_q = \begin{cases} \frac{1}{\sqrt{N}}, & \text{if } q = 0. \\ \sqrt{\frac{2}{N}}, & \text{if } 1 \leq q \leq N - 1. \end{cases} \quad (3.7)$$

In the proposed method, instead of taking all the DCT coefficients of a block, few low frequency coefficients are chosen. It is obvious that if all of the DCT coefficients were used, it would definitely result in a feature vector with a very large dimension. As DCT exhibits energy compactness property, first few DCT coefficients carry most of the energy of the block centered on the candidate pixel  $(x, y)$ . Hence, first 4 DCT coefficients are used in the feature vector.

In Fig. 3.15, Fig. 3.16, Fig. 3.17 and Fig. 3.18, histograms computed for vessel pixels (left figure) and non-vessel pixels (right figure) corresponding to the first four DCT coefficients of the block are shown, respectively. It is observed from these figures that there exists significant overlap between the two classes. These overlapping features affect the proper representation of a pixel, which will increase the chances of misclassification. Therefore, use of spectral feature alone may not be a good solution. Rather it may be used along with some other features.

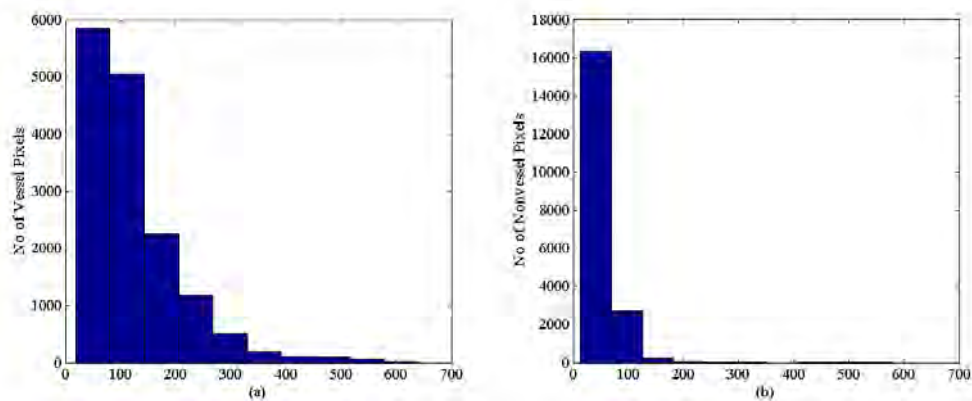


Fig. 3.15: Histograms computed for vessel pixels (left figure) and non-vessel pixels (right figure) corresponding to the first DCT coefficient of the block.

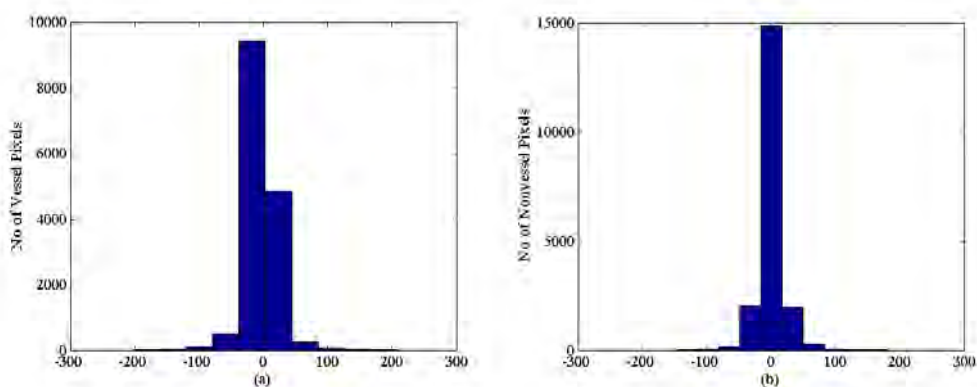


Fig. 3.16: Histograms computed for vessel pixels (left figure) and non-vessel pixels (right figure) corresponding to the second DCT coefficient of the block.

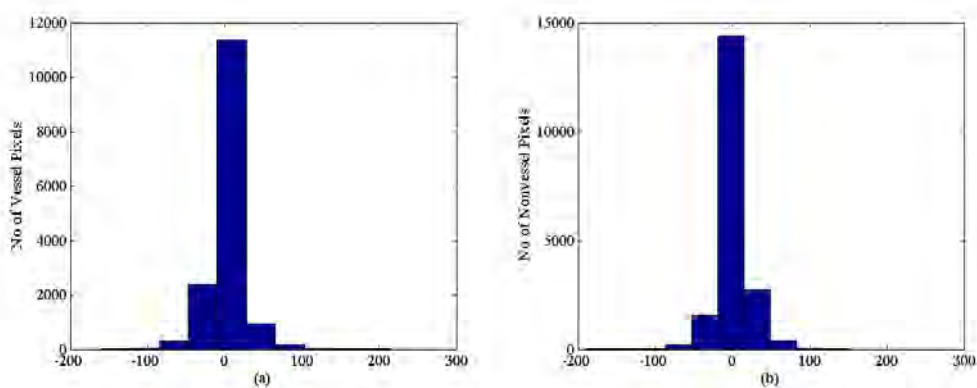


Fig. 3.17: Histograms computed for vessel pixels (left figure) and non-vessel pixels (right figure) corresponding to the third DCT coefficient of the block.

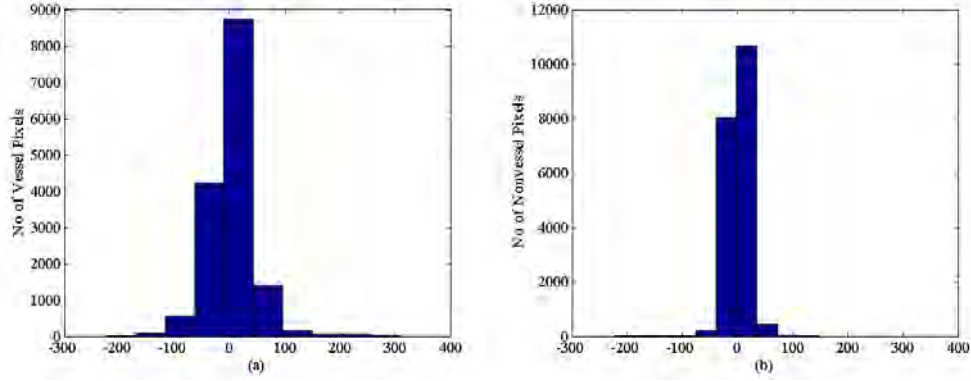


Fig. 3.18: Histograms computed for vessel pixels (left figure) and non-vessel pixels (right figure) corresponding to the first DCT coefficient of the block.

### 3.2.3 Choice of Spatial Block Size

One major concern in extracting feature from a spatial block is the size of the block. From statistical point of view, larger the block size better the statistical properties to be extracted from a block. For example the mean or the min-max operators used in spatial feature extraction can provide consistent and representative values when large variations are taken into consideration. However, these facts strongly depend on the specific application. Since the width of the vessel is very small (generally 3 to 5 pixels) in comparison to the entire retinal image, considering large block may not represent unique characteristics in this application. Given a pixel  $(x, y)$  of the vessel-enhanced image  $I_{VE}$ , a square block  $S_{x,y}^{\omega}$  centered at  $(x, y)$  is considered for spatial feature extraction, where the block size  $\omega \times \omega$  is varied from  $3 \times 3$  to  $9 \times 9$ . However, it is experimentally found that larger block size not only increases the computational burden but also provides inconsistent features. In the proposed method,  $5 \times 5$  block size is found to be suitable.

### 3.2.4 Feature Quality

Fig. 3.19, Fig. 3.20 and Fig. 3.21 indicate within class compactness of the statistical spatial features proposed. X-axis indicates different features and along Y-axis, feature value of both vessel and nonvessel pixels have been placed on the same plot.

It is expected that for a good feature, one class will be concentrated in one height and the other in another height and for each case they are densely placed,



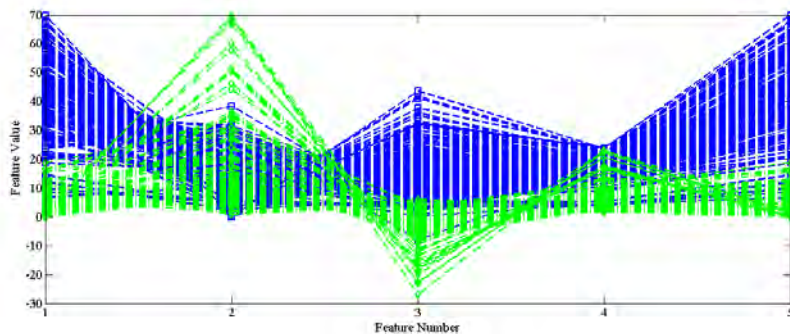


Fig. 3.19: Within Class Compactness. X-axis Dimension: (1)-(5) Five Spatial Features. Blue and green color refer to vessel and nonvessel pixels respectively.

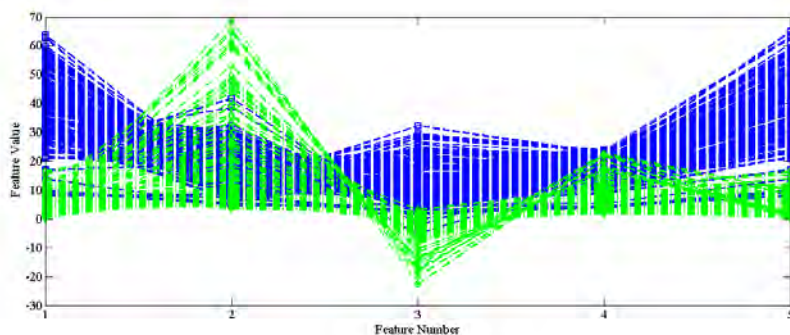


Fig. 3.20: Within Class Compactness. X-axis Dimension: (1)-(5) Average of Five Spatially Shifted Statistical Features. Blue and green color refer to vessel and nonvessel pixels respectively.

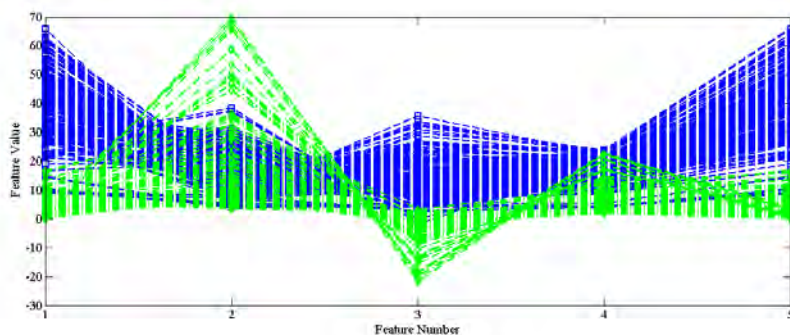


Fig. 3.21: Within Class Compactness. X-axis Dimension: (1)-(5) Median of Five Spatially Shifted Statistical Features. Blue and green color refer to vessel and nonvessel pixels respectively.

but two classes are separated. And each of the figures Fig. 3.19, Fig. 3.20 and Fig. 3.21 depicting feature quality properly follow these criteria. Both their within class compactness and between class separability are high. It can be assumed that these particular features are bound to perform well.

In 3.22, Fig. 3.23 and Fig. 3.24, X-axis indicates different features and along

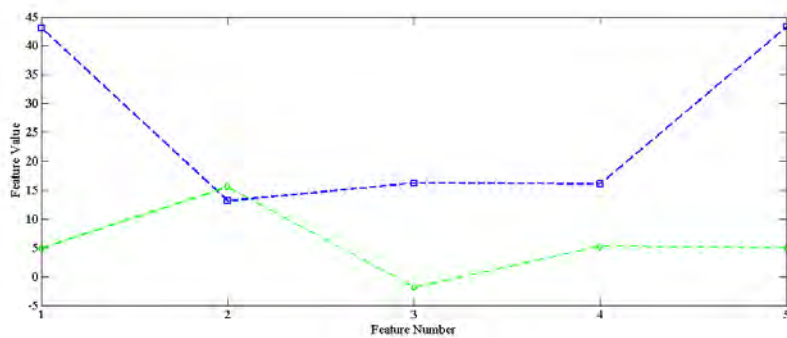


Fig. 3.22: Between Class Separability. X-axis Dimension: (1)-(5) Centroid of Five Spatial Features. Blue and green color refer to vessel and nonvessel pixels respectively.

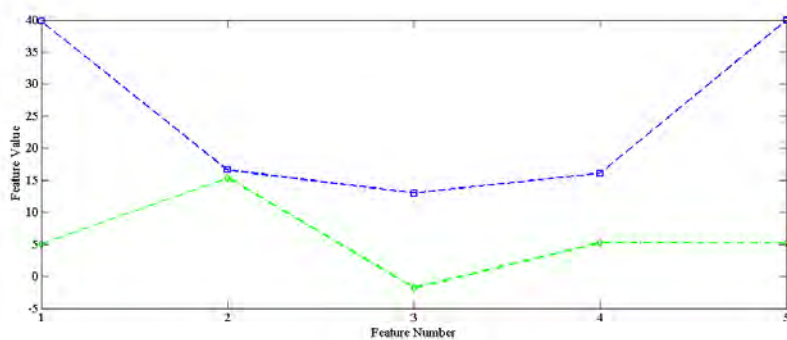


Fig. 3.23: Between Class Separability. X-axis Dimension: (1)-(5) Centroid of Average of Five Spatially Shifted Statistical Features. Blue and green color refer to vessel and nonvessel pixels respectively.

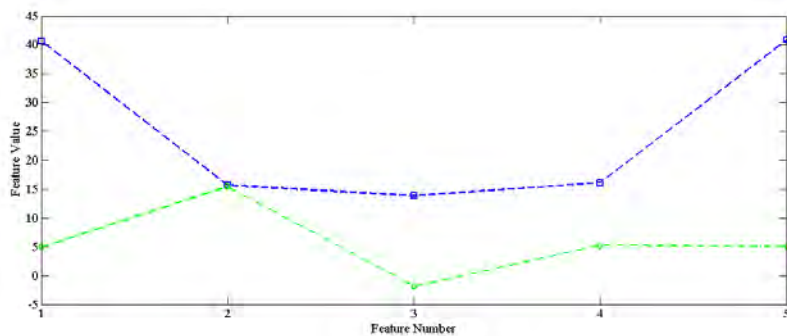


Fig. 3.24: Between Class Separability. X-axis Dimension: (1)-(5) Centroid of Median of Five Spatially Shifted Statistical Features. Blue and green color refer to vessel and nonvessel pixels respectively.

Y-axis, centroid of each feature of both vessel and nonvessel pixels have been placed on the same plot. These figures also indicate the high between class separability of each of the proposed features.

### 3.3 Train Formation

One of the major task in supervised classification is to develop a training dataset, which has direct impact on the classification performance. Training dataset is generally a representative set of data which helps to take decision about the class label of a test sample. Hence, designing a training dataset is not a trivial task. Train formation or trainer pixel selection for vessel pixel classification can be executed in two different ways:

- **Conventional Manual Approach**
- **Proposed Connectivity Based Approach**

#### 3.3.1 Conventional Manual Approach

The most common approach of developing train set is the manual selection based on previous knowledge and judgment. It is mainly an eye inspection method for training pixel selection. In this case, during the training data selection process, the objective is to obtain as much variation as possible. The train dataset can be made more representative for the unknown test dataset by proper insertion of data that contain characteristics similar to test samples. In the case of vessel pixel classification, accuracy can definitely be improved if pixels similar to misclassified confusing test samples can be trained. If manually this task can be performed and pixels are picked up carefully so that they are able to represent all the test samples, classifier will perform well and give excellent results. This manual selection is followed in all the previously reported retinal pixel classification methods, such as [21]. The major problem in this method is that, since it is training dependent and train is prepared considering test samples of a particular database, this train data cannot perform well for all other databases universally. Therefore, in our proposed method, a universal rule is devised, which is expected to perform well for all standard databases of retinal images.

#### 3.3.2 Proposed Connectivity Based Train Set Design

Instead of manual selection of trainer pixels by eye inspection as described in the previous subsection, an automatic train set design procedure is devised based on

connectivity measurement of a candidate pixel. Connectivity of a candidate pixel is defined as the number of vessel pixels present in a spatial block. Proposed connectivity based trainer design can be divided into two different approaches:

1. Trainer design for all candidate classification
2. Trainer design for critical candidate classification

Among the two databases (DRIVE and STARE), only DRIVE database provides a separate train dataset. Hence for train data selection, train images provided by the DRIVE database are used.

### Trainer Design for All Candidate Selection

In this approach, all vessel candidates, selected in the gradient search based vessel detection method, are classified further as vessel or non-vessel. Vessel candidates obtained from the gradient based method can be classified into three categories:

- **Strong vessel pixels:** Located almost along the midline of a vessel
- **Weak vessel pixels:** Located at the edge of a vessel
- **Weak non-vessel pixels:** Located at the outside margin of a vessel

Based on this assumption, the output vessel pixels of the search method are further analyzed on the basis of connectivity. It is curiously observed that these pixels can be divided into five precise categories:

1. Strong vessel pixels:  $V_{25} = 25, 26 \leq V_{49} \leq 49, C_P = VesselPixel$
2. Less strong vessel pixels:  $V_9 = 9, 12 \leq V_{25} < 25, C_P = VesselPixel$
3. Weak vessel pixels:  $2 \leq V_9 \leq 8, C_P = VesselPixel$
4. Weak non-vessel pixels:  $1 \leq V_9 \leq 8, C_P = NonvesselPixel$
5. Less weak non-vessel pixels:  $V_9 = 9, 12 \leq V_{25} < 25, C_P = NonvesselPixel$

Here,  $V_{49}$ =Connectivity of a pixel inside a  $7 \times 7$  window centered on it

$V_{25}$ =Connectivity of a pixel inside a  $5 \times 5$  window centered on it

$V_9$ =Connectivity of a pixel inside a  $3 \times 3$  window centered on it

For non-vessel pixels defined by third and fourth criteria, connectivity refers to total number of non-vesel pixels around each of the pixel.

Therefore, in the design of the proposed train set, following five types of vessel pixels are selected.

1. Strong vessel pixels:  $V_{25} = 25$ ,  $34 \leq V_{49} \leq 49$ ,  $C_P = VesselPixel$
2. Less strong vessel pixels:  $V_9 = 9$ ,  $14 \leq V_{25} < 25$ ,  $C_P = VesselPixel$
3. Weak vessel pixels:  $5 \leq V_9 \leq 8$ ,  $14 \leq V_{25} < 25$ ,  $C_P = VesselPixel$
4. Weak non-vessel pixels:  $5 \leq V_9 \leq 8$ ,  $14 \leq V_{25} < 25$ ,  $C_P = NonvesselPixel$
5. Less weak non-vessel pixels:  $V_9 = 9$ ,  $14 \leq V_{25} < 25$ ,  $C_P = NonvesselPixel$

Fig. 3.25 shows the selected pixel types.

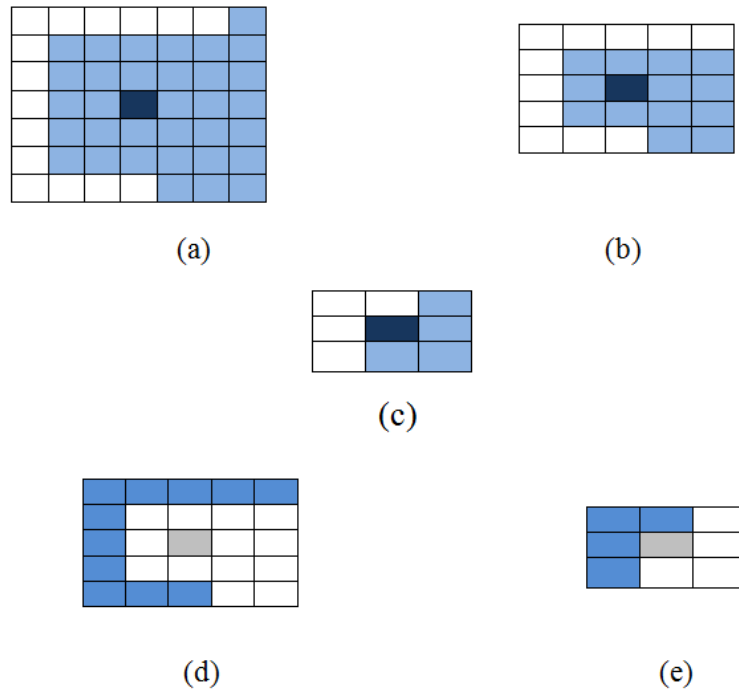


Fig. 3.25: Selected pixel types. (a) Strong vessel, (b) less strong vessel, (c) weak vessel, (d) less weak nonvessel, and (e) weak non-vessel. Pixel selection criteria: blue and white color indicate vessel and nonvessel pixels respectively. Dark blue and ash colored pixels indicate vessel and nonvessel center pixel accordingly.

### Trainer Design for Critical Candidate Selection

Instead of classifying all candidate pixels selected in search method, based on the proposed criterion of connectivity of each candidate pixel estimated from the output

binary image, some candidate pixels are confirmed as vessel pixel and excluded from classification procedure. Candidate pixels with following characteristics are regarded as sure to be vessel pixel:

- $V_{25} = 25, 26 \leq V_{49} \leq 49$
- $V_9 = 9, 20 \leq V_{25} < 25$
- $V_9 = 8, 19 \leq V_{25} < 25$

All other candidate pixels without above conditions are then considered as critical candidate, since they have greatly overlapping characteristics between vessel and non-vessel categories. Therefore in the second approach, while choosing trainer pixels, search method is applied on the trainer images and output pixels having a connectivity estimated from the output binary image below 12 within a  $5 \times 5$  block centered on it with minimum two non-vessel pixel inside  $3 \times 3$  window around it, are first selected. These pixels have a vessel connectivity ranging from 1 to 7 within a  $3 \times 3$  block around them. Therefore these pixels can be categorized into seven classes.

1.  $V_9 = 1$
2.  $V_9 = 2$
3.  $V_9 = 3$
4.  $V_9 = 4$
5.  $V_9 = 5$
6.  $V_9 = 6$
7.  $V_9 = 7$

Then based on a ‘score’, the selected pixels are sorted in a descending order and a definite number of first few pixels are chosen from each connectivity category proportioned by thorough observation of each trainer image as trainer pixels grouping them with the help of labels acquired from ground truth of those trainer images.

$$S = 10 \times C + P_i \quad (3.8)$$

Here  $C$ =Connectivity of a pixel within a  $5 \times 5$  block centered on it and  $P_i$ =pixel intensity obtained from the preprocessed image and  $S$ =Score

### 3.3.3 Train Image Selection

While selecting train pixels, five train images are considered from the given Train database of twenty images in the standard DRIVE database. In fact, all given train images have been tested, but it is found that not all training images are well represented. Training images are categorized and then one is selected from each category. Again, one may select training pixels from all images, it is found that including pixels from many images degrades the distinguishing difference between two classes, since higher the number of train images may not necessarily enhance trainer quality, that may provide redundant or biased trainer. Therefore, one train image is selected from different categories of images and the final number of images becomes five.

## 3.4 Classification

The problem of retinal vessel detection is formulated as a supervised classification problem. In case of supervised classification, generally some training data with known class index are available. Based on the characteristics of the train data, the unknown test sample needs to be classified. Here the classification problem deals with two class problems, vessel and non-vessel. During the test phase, K-fold cross validation technique is most widely used to analyze the performance of a classification scheme. The classification performance is tested by using different classifiers, such as distance based classifier, k nearest neighborhood classifier (kNN) and linear discriminant analysis (LDA). However, considering the robustness of classifier along with the computational complexity, LDA is found most suitable in the proposed vessel classification scheme. Next, basic principle of the LDA classifier is explained.

### 3.4.1 Linear Discriminant Based Classifier (LDA)

A classifier that is based on maximal separation of centroids, suffers from a drawback that it does not take into account the second-order statistics of data distribution fully. In order to mitigate this problem, a more effective classification algorithm is

Fisher's LDA which takes into account the intra-cluster scatter matrix computed from the training vectors relating to each of the two classes. In LDA, the scatter matrix is a scaled covariance matrix and defined as (3.9).

$$S = \sum_{i=1}^N [x_i - \mu][x_i - \mu]^T, \quad (3.9)$$

where  $\mu$  denotes the global mean of the entire set of the training vector. The between-class scatter matrix is denoted as (3.10)

$$S_b = N_+[\mu_+ - \mu][\mu_+ - \mu]^T + N_-[\mu_- - \mu][\mu_- - \mu]^T \quad (3.10)$$

Here the three points, namely  $\mu$ ,  $\mu_+$  and  $\mu_-$  are collinear, meaning that

$$[\mu_+ - \mu] = \frac{N_-}{N}[\mu_+ - \mu_-] \quad (3.11)$$

and

$$[\mu_- - \mu] = -\frac{N_+}{N}[\mu_+ - \mu_-]. \quad (3.12)$$

Using the values obtained from (3.11) and (3.12) in (3.10), the between class scatter matrix is obtained as (3.13)

$$S_b = \frac{N_-N_+}{N}[\mu_+ - \mu_-][\mu_+ - \mu_-]^T. \quad (3.13)$$

In addition, the within class scatter matrix is defined as (3.14)

$$S_w = \sum [x_i - \mu_+][x_i - \mu_+]^T + \sum [x_i - \mu_-][x_i - \mu_-]^T. \quad (3.14)$$

The goal of LDA is to find out the linear projection  $w_{opt}$  using these relationships which maximize a special kind of signal to noise ratio. Here the signal is represented by the projected inter-cluster distance and the noise by the projected intra-cluster variance. The objective function is based on determining a projection direction  $w$  to maximize the Fisher's discriminant defined as (3.15).

$$J(w) = \frac{w^T S_b w}{w^T S_w w} \quad (3.15)$$

### 3.5 Results and Analysis

In order to quantify the algorithmic performance of the proposed method of pixel classification on a fundus image, the resulting segmentation is compared to its corresponding gold-standard image discussed in the result section of the previous chapter.



In this chapter, our algorithm of vessel candidate classification is evaluated in terms of sensitivity  $Se$ , specificity  $Sp$ , positive predictive value  $Ppv$ , negative predictive value  $Npv$ , and accuracy  $Acc$ . Taking Table 2.1 into account, these metrics are defined by Eqn. (2.4), Eqn. (2.5), Eqn. (2.6), Eqn. (2.7) and Eqn. (2.8) described in the previous chapter. The proposed method is evaluated on DRIVE and STARE database images with available gold-standard images. The retinal pixel classification scheme proposed in this chapter consists of two stages: (1) candidate vessel detection by using the gradient based search method on enhanced retinal image and (2) supervised classification which involves three major steps: (i) training data set development, (ii) critical candidate selection, (iii) proposed feature extraction and (iv) LDA based candidate vessel classification into two class: vessel and non-vessel. The first stage is exactly the same method described in the last chapter. Different steps involved in second stage are described in this chapter.

### 3.5.1 Performance Evaluation

At first, classification is performed on all pixel candidates obtained in gradient based search method with  $N_p = 5$  (since this threshold provides best candidates as compared to any other threshold) on both DRIVE and STARE databases. Results are shown in Table 3.2 and Table 3.3, respectively.

Next, the classification task is carried out only on critical candidates from both DRIVE and STARE databases. Results of this action are presented in Table 3.4 and Table 3.5. It is observed that all candidate classification does not provide accuracy as good as critical candidate classification does for DRIVE database images, average accuracy improves significantly from 93.89% to 94.23%. But in case of STARE database, the consequences are opposite. All candidate classification provides an average accuracy of 95.16% while the other one cannot give more than 94.95%.

Table 3.6 shows a comparison between gradient based search and vessel candidate classification. It also provides an opportunity to clearly observe the improvement of accuracy due to applying classification approach to the candidates selected in search method. Fig. 3.26 provides the manual labeling and output binary images for Gradient based search and both classification approaches made to an image from DRIVE database. It can be concluded from the results given in Table 3.2, Table

Table 3.2: Performance metrics obtained by using the proposed method on DRIVE database

<b>Image</b>	<i>Se</i>	<i>Sp</i>	<i>Ppv</i>	<i>Npv</i>	<i>Acc in percentage</i>
1	0.6558	0.9875	0.8876	0.9500	94.40
2	0.6733	0.9906	0.9265	0.9451	94.30
3	0.4991	0.9952	0.9469	0.9210	92.30
4	0.6133	0.9932	0.9324	0.9435	94.25
5	0.5203	0.9965	0.9587	0.9297	93.19
6	0.4977	0.9968	0.9623	0.9235	92.64
7	0.5614	0.9917	0.9116	0.9368	93.47
8	0.4534	0.9947	0.9247	0.9268	92.6654
9	0.4905	0.9965	0.9486	0.9363	93.70
10	0.5598	0.9935	0.9211	0.9433	94.17
11	0.6009	0.9883	0.8843	0.9433	93.81
12	0.5544	0.9929	0.9179	0.9397	93.80
13	0.5452	0.9940	0.9376	0.9297	93.04
14	0.6358	0.9878	0.8745	0.9530	94.63
15	0.6528	0.9821	0.8083	0.9606	94.79
16	0.5947	0.9922	0.9195	0.9421	94.02
17	0.5385	0.9926	0.9115	0.9386	93.66
18	0.6078	0.9870	0.8583	0.9510	94.34
19	0.6828	0.9951	0.9506	0.9582	95.75
20	0.5750	0.9922	0.8982	0.9514	94.77
<i>Avg</i>	0.5429	0.9920	0.9140	0.9411	93.89

3.3, Table 3.4 and Table 3.5 that only critical candidate classification gives better accuracy for both DRIVE and STARE databases than that provided by gradient based search method.

### **Effect of classifier**

Table 3.7 provides performance of other classifiers rather than two-class LDA in case of three images of DRIVE database where Image 15 is the best case of this database, Image 3 worst case, and Image 1 is a general case of reflecting the performance criteria of the proposed method classifier.

Here,

DLDA=Diaglinear Discriminant Analysis Classifier

DQDA=Diagquadratic Discriminant Analysis Classifier

NB=Naive Bayes classifier

KNN=K-Nearest Neighborhood Classifier

Table 3.3: Performance metrics obtained by using the proposed method on STARE database

<b>Image</b>	<i>Se</i>	<i>Sp</i>	<i>Ppv</i>	<i>Npv</i>	<i>Acc in percentage</i>
1	0.4742	0.9876	0.8234	0.9390	93.18
2	0.4703	0.9851	0.7706	0.9459	93.56
3	0.7101	0.9724	0.6974	0.9740	95.08
4	0.2033	0.9993	0.9730	0.9149	91.61
5	0.6548	0.9766	0.7999	0.9519	93.64
6	0.7710	0.9781	0.7751	0.9776	95.97
7	0.8127	0.9692	0.7655	0.9767	95.20
8	0.7897	0.9773	0.7999	0.9759	95.80
9	0.7767	0.9791	0.8180	0.9732	95.73
10	0.6818	0.9804	0.8127	0.9611	94.73
11	0.7803	0.9826	0.8312	0.9760	96.26
12	0.8542	0.9776	0.8203	0.9825	96.44
13	0.7338	0.9822	0.8523	0.9635	95.18
14	0.7214	0.9848	0.8722	0.9610	95.18
15	0.6173	0.9879	0.8732	0.9504	94.39
16	0.4195	0.9944	0.9261	0.9115	91.24
17	0.7016	0.9917	0.9225	0.9592	95.57
18	0.4846	0.9980	0.9497	0.9622	96.18
19	0.4304	0.9965	0.8840	0.9658	96.34
20	0.4240	0.9922	0.8469	0.9440	93.95
<i>Avg</i>	0.6256	0.9847	0.8407	0.9583	95.16

This comparison concludes that LDA is the best classifier showing moderately good performance in most of the cases.

### **Effect of feature dimension reduction**

Fig. 3.27 shows effect of feature dimension variation for a test image of DRIVE database. It is observed that with increase in features, accuracy also increases. The best accuracy occurs when all features are included. For this particular test image, inclusion of spectral features increases accuracy, but for most of the test images, accuracy is decreased resulting in drastic fall in Sensitivity (*Se*).

### **Effect of Retraining**

It has been mentioned that train images were selected from standard DRIVE database after rigorous trials and observation such that the selected images provide the best average accuracy possible for the whole set of test images. During trials, it is ob-

Table 3.4: Performance metrics obtained by using the proposed method on DRIVE database for critical pixel classification

<b>Image</b>	$Se$	$Sp$	$Ppv$	$Npv$	<i>Acc in percentage</i>
1	0.7116	0.9825	0.8596	0.9576	94.70
2	0.7297	0.9844	0.8916	0.9539	94.62
3	0.5452	0.9923	0.9232	0.9275	92.71
4	0.6703	0.9891	0.9042	0.9512	94.66
5	0.5688	0.9942	0.9393	0.9363	93.65
6	0.5499	0.9941	0.9385	0.9308	93.14
7	0.6151	0.9872	0.8802	0.9438	93.80
8	0.5099	0.9911	0.8920	0.9336	93.06
9	0.5708	0.9928	0.9131	0.9456	94.32
10	0.6045	0.9907	0.8982	0.9486	94.46
11	0.6573	0.9827	0.8499	0.9506	94.05
12	0.6129	0.9893	0.8915	0.9470	94.22
13	0.5968	0.9900	0.9076	0.9370	93.42
14	0.6924	0.9809	0.8292	0.9598	94.69
15	0.7096	0.9763	0.7762	0.9667	94.86
16	0.6565	0.9881	0.8924	0.9503	94.47
17	0.6034	0.9891	0.8866	0.9466	94.16
18	0.6627	0.9823	0.8296	0.9573	94.56
19	0.7373	0.9915	0.9224	0.9650	96.09
20	0.6254	0.9886	0.8680	0.9567	94.99
<i>Avg</i>	0.6315	0.9879	0.8847	0.9483	94.23

served that if a different set of five train images are selected, that set of train provides worse result for some images, but much better for others. It is found that such a set provides an accuracy of 95.11% for a particular test image of DRIVE database which previously for the selected set of train images was 94.86%. But for another image, this set provides 92.10% which previously was 92.71%. Therefore it can be concluded that classification result is mostly train dependent. If manual selection by eye inspection as done in [21] is performed also in the proposed method in this chapter, it definitely will increase the vessel detection accuracy. But the target of the proposed method is to devise a universal rule of train selection which will perform well independently for any retinal image of any standard database.

### **Effect of Inclusion of Some Nonvessel Candidates for Classification**

Classification method is also observed for some pixels which were not selected as vessel candidates in the search method, but are in the neighborhood of those selected

Table 3.5: Performance metrics obtained by using the proposed method on STARE database for critical pixel classification

<b>Image</b>	$Se$	$Sp$	$Ppv$	$Npv$	<i>Acc in percentage</i>
1	0.5000	0.9843	0.7949	0.9417	93.16
2	0.4974	0.9828	0.7541	0.9484	93.61
3	0.7296	0.9678	0.6702	0.9756	94.82
4	0.2441	0.9987	0.9552	0.9188	91.98
5	0.7063	0.9669	0.7529	0.9584	93.43
6	0.8156	0.9691	0.7204	0.9818	95.54
7	0.8292	0.9609	0.7241	0.9785	94.64
8	0.7951	0.9717	0.7635	0.9763	95.35
9	0.7911	0.9726	0.7770	0.9747	95.3
10	0.6939	0.9725	0.7584	0.9623	94.16
11	0.8152	0.9740	0.7751	0.9796	95.83
12	0.8793	0.9686	0.7701	0.9853	95.90
13	0.7610	0.9769	0.8216	0.9670	95.05
14	0.7493	0.9788	0.8353	0.9645	94.99
15	0.6414	0.9836	0.8405	0.9531	94.29
16	0.4302	0.9931	0.9125	0.9129	91.28
17	0.7485	0.9857	0.8811	0.9652	95.63
18	0.5391	0.9968	0.9268	0.9660	96.44
19	0.5108	0.9946	0.8539	0.9704	96.63
20	0.4883	0.9877	0.8020	0.9497	94.14
<i>Avg</i>	0.6583	0.9794	0.8045	0.9615	94.95

candidates. This was done with the hope that it may increase the accuracy by including some true vessel pixels which were discarded in the search method. But this inclusion has no effect, for Image 3 of DRIVE database, where number of ‘False Negative’ is too high, this job is done without resulting in any improvement. This is because the true vessel pixels discarded as ‘False Negative’ in search method, are those far from the neighborhood of selected candidates and mostly are thin vessel pixels. There is no possible way of including them in classification procedure with search based on mere connectivity measure. Therefore, only vessel candidates are

Table 3.6: Comparison between gradient based search method and vessel pixel classification

<b>Database</b>	<b>Search</b>	<b>Classification (All)</b>	<b>Classification (Critical)</b>
<b>DRIVE</b>	93.9073	93.89	94.23
<b>STARE</b>	93.9109	95.16	94.95

Table 3.7: Comparison Among Different Classification Methods In Terms Of Accuracy

<b>Classifier</b>	<b>Image 1</b>	<b>Image 3</b>	<b>Image 15</b>
<b>LDA</b>	94.70	92.71	94.86
<b>DLDA</b>	94.67	92.58	94.80
<b>DQDA</b>	94.67	92.60	94.79
<b>NB</b>	94.68	92.71	94.73
<b>KNN</b>	94.70	92.96	94.52

further dealt with.

### 3.5.2 Comparison to Other Methods

Table 3.8 provides comparison of the performance of the proposed method in terms of average accuracy to other methods. It is observed that the accuracy of the proposed method is comparable with those of other papers. However, the novelty and simplicity of both proposed methods are quite noticeable. The simple and vastly competent search algorithm used in the gradient based search method, easily formulated and computed features and the universal trainer selection algorithm employed in the supervised classification method depict the efficiency of them over the other methods.

Table 3.8: Performance Metrics Compared To Other Methods On The Stare And Drive Databases In Terms Of Average Accuracy

<b>Method Type</b>	<b>Method</b>	<b>DRIVE</b>	<b>STARE</b>	<b>DRIVE+STARE</b>
<b>Supervised</b>	Staal <i>et al.</i> [18]	0.9441	–	–
	Niemeijer <i>et al.</i> [17]	0.9417	–	–
	Soares <i>et al.</i> [19]	0.9466	0.9480	0.9473
	Ricci and Perfetti [20]	0.9595	0.9646	0.9621
	Marin <i>et al.</i> [21]	0.9452	0.9526	0.9489
	Proposed Method	0.9423	0.9495	0.9459
<b>Ruled-Based</b>	Chaudhuri <i>et al.</i> [7]	0.8773	–	–
	Hoover <i>et al.</i> [23]	–	0.9275	–
	Jiang and Mojon [9]	0.8911	0.9009	0.8960
	Mendonça <i>et al.</i> [6]	0.9463	0.9479	0.9471
	Martinez-Perez <i>et al.</i> [12]	0.9344	0.9410	0.9377
	Cinsdikici and Aydin [8]	0.9293	–	–
	Proposed Method	0.9390	0.9391	0.939

### 3.5.3 Processing Times

It is observed that the superiority of the proposed schemes over other algorithms tested using the DRIVE database is in the time requirement to process an image with appreciable accuracy. Computational time for the MATLAB implementation of the proposed gradient based vessel detection algorithm tested on a DRIVE database image requires approximately 1.83 s second to process. Table 3.9 shows that the proposed gradient based search method requires in average a time of only 1.83 s which is slightly higher than only one method so far available in literature [14] but it provides comparatively higher accuracy.

Proposed classification method provides a very lower computational time at the cost of slightly lower accuracy as compared to other supervised classification methods, such as [19] and [18]. Though Table 3.9 does not provide computational time for [21], it was attempted to make an assumption of timing for the method proposed here. It is found that in order to extract feature for only 4596 number of pixels, the method requires 22.819s whereas for pixel by pixel classification, about 3,30,000 number of pixels need feature extraction. Therefore only feature extraction requires a huge computational time according to [21]. These results compare favorably with timings reported for most of the other algorithms in terms of higher accuracy and lower computation time.

Table 3.9: Time requirements by different vessel detection algorithms. Here, Impl=Implementation, M=MATLAB

Method	Processor	RAM	Impl	Accuracy	Time
Bankhead [14]	2.13 GHz	2 GB	M	0.9371	0.093 s
Espona [11]	1.83 GHz	2 GB	C++	0.9352	38.4 s
Mendonca [6]	3.2 GHz	960 MB	M	0.9463	< 150 s
Soares [19]	2.1 GHz	1 GB	M	0.9466	180 s
Staal [18]	1 GHz	1 GB	M	0.9441	900 s
Proposed(Search)	2.5 GHz	2 GB	M	0.9390	1.830 s
Proposed(Classification)	2.5 GHz	2 GB	M	0.9423	13.114 s

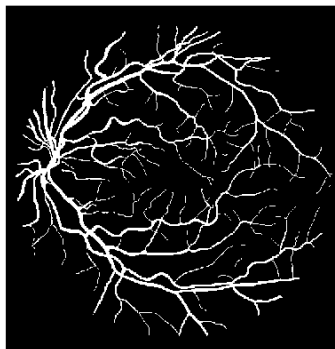
Again, it has been experimented that with reduction in the number of features in the proposed method of vessel candidate classification, we could drastically reduce computational time by negotiating accuracy. For example, the processing time for the first image of the DRIVE database would reduce to 7.051 s from 16.046 s and the

accuracy would reduce from 94.70% to 94.58%. For the second image, the accuracy would fall from 94.62% to 94.56% with a drastic fall in processing time from 16.777 s to 5.011 s.

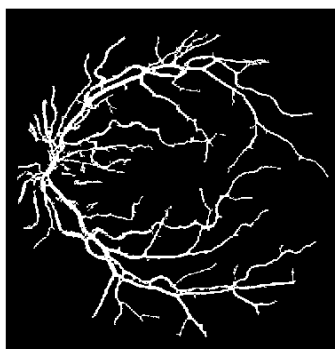
### **3.6 Conclusion**

In this chapter, a supervised classification method is proposed incorporating a pre-processing algorithm, feature extraction of the preprocessed image, universal train formation and linear discriminant based classifier. For preprocessing, background subtraction based shade correction and sequential opening filtering prior to Top-Hat transform is employed. For pixel representation, statistical spatial features, shifted statistical spatial features and spectral features are extracted. A novel universal train selection algorithm is proposed employing separate approaches made to all vessel candidates obtained in search method and only critical vessel candidates. Train pixels are selected according to this algorithm from train images provided by standard DRIVE database. Finally a linear discriminant based classifier is applied to retinal images of standard databases to classify the vessel candidates of each image those are already extracted by gradient based search method. It is found that the proposed method requires significantly less computational time to perform the classification task with a very competitive overall classification accuracy.

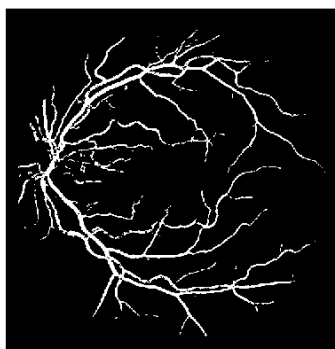




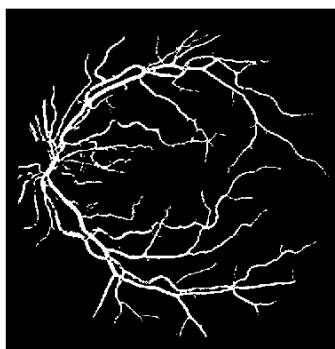
(a)



(b)



(c)



(d)

Fig. 3.26: An example of binary output image of classification. (a) Manual labeling, (b) search output, (c) all candidate classification output and (d) critical candidate classification output

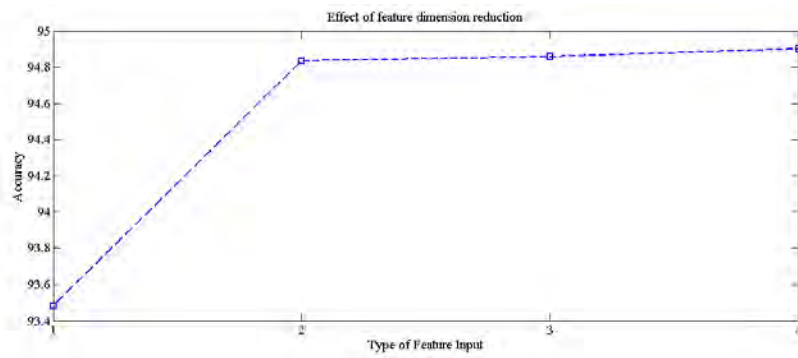


Fig. 3.27: Effect of feature dimension reduction on a Particular Image. X-axis Dimension: 1) 2-D DCT Coefficients 2) 5 Spatial Features 3) Proposed Spatial and Shifted Spatial Features 4) All considered Features.

# Chapter 4

## Conclusion

### 4.1 Contribution of this Thesis

- The main objective of this thesis work is to develop a fast and efficient blood vessel detection technique for retinal images. In order to achieve this target, two different schemes are proposed, one falls in the category of rule based approach and the other one is the supervised classification approach. The objective of the first scheme is to provide satisfactory vessel detection performance with a very low computational cost of processing the whole image. Prior to vessel detection, preprocessing is required for any RGB retinal image in order to obtain spatially enhanced image free from background noise and lightning variations. That is to bring down all the images to be tested on the same platform. One major contribution is to introduce an efficient preprocessing scheme consisting of adaptive median filtering and Top-Hat transform. In this regards, the idea of repeated median filtering is also introduced. Consequently, an appropriate enhanced image is obtained.
- An intensity gradient based search algorithm is proposed for vessel detection from enhanced retinal image. The intensity level of the candidate pixel is compared with those of three consecutive pixels along with the previous pixel, and if the difference exceeds a definite threshold in each case, depending on the polarity of the difference, the pixel as well as the neighboring pixel, is declared as vessel or non-vessel. This method is fast, uncomplicated and competent to provide itself an acceptable accuracy in blood vessel detection.
- The second scheme proposed in this thesis performs the feature based vessel

classification from a set of given vessel candidates. In order to reduce the number of ‘False Positive’, vessel candidates selected in the gradient search method are further classified extracting suitable features and employing a suitable classifier incorporating efficient trainer pixels. The first task of classification is extraction of competent features to represent efficiently a particular pixel. In this purpose, along with some spatial statistical features extracted from the spatial mask centered on the candidate pixel to be classified, additional spatially shifted masks are utilized to provide a proper gray level description in the neighborhood of the candidate pixel. These proposed features along with spatial features of the center mask are observed to represent vessel pixels from the non-vessel ones with proper distinction, which is actually required for an efficient classification.

- For efficient feature extraction from retinal image, preprocessing is required. In the gradient based search method, the nature of the pixel is determined with the help of a certain neighborhood. But in pixel classification, which is completely a different method, small spatial block around a pixel is taken into account for feature extraction. Therefore, preprocessing required here must be adaptable with this method. Bearing that in mind, an efficient preprocessing scheme is developed incorporating shade correction with background subtraction and sequential opening operation prior to Top-Hat transform. This method is found to be very effective to provide a suitably enhanced image.
- In the proposed vessel candidate classification method, a universal train selection algorithm is proposed. Based on a connectivity measure, train pixels are selected automatically. While selecting train pixels, pixels with similar connectivity measurement are chosen. In a different approach of train selection, only critical candidates (candidates having greatly overlapping characteristics between vessel and non-vessel categories) are considered. In this approach, instead of classifying all candidates, only some critical candidates situated along the edge of a vessel are taken into classification process. For them, suitable train pixels are chosen through an automated process by applying search method to train images and accepting pixels as train pixels which fulfill the connectivity criteria of critical candidates from the output binary image of

the search method and also get sorted based on a score defined by the pixel neighborhood along with the intensity value of the pixel itself.

- As an application of the proposed blood vessel detection scheme, vessel recognition scheme is also developed based on linear discriminant analysis. It is observed that the application of vessel candidate selection reduces the computational cost and processing time in comparison to some of the existing methods. On the other hand, employment of the classification process on the selected candidates reduces ‘False Positive’s detected earlier resulting in a better accuracy.

## 4.2 Scope and Future Work

- One possible future work could be to make the vessel candidate selection process stronger by including more candidates, since classification procedure has no scope to work on the vessel pixels declared as non-vessel already in the search method.
- Another future work could be to investigate higher order statistical features on spatial blocks in order to differentiate between critical vessel and non-vessel pixels so that some true vessel pixels are not excluded as being misclassified, which may further increase the vessel detection accuracy to the maximum possible extent.

# Bibliography

- [1] M. Niemeijer, B. van Ginneken, J. J. Staal, M. S. A. Suttorp-Schulten, and M. D. Abramoff, “Automatic detection of red lesions in digital color fundus photographs,” *IEEE Trans. Med. Imag.*, vol. 24, no. 5, pp. 584–592, May 2005.
- [2] A. J. Frame, P. E. Undrill, M. J. Cree, J. A. Olson, P. F. S. K. C. McHardy, and J. V. Forrester, “A comparison of computer based classification methods applied to the detection of microaneurysms in ophthalmic fluorescein angiograms,” *Comput. Biol. Med.*, vol. 28, no. 3, pp. 225–238, May 1998.
- [3] O. Chutatape, L. Zheng, and S. Krishman, “Retinal blood vessel detection and tracking by matched gaussian and kalman filters,” in *IEEE Int. Conf. Eng. Biol. Soc.*, vol. 20, 1998, pp. 3144–3149.
- [4] L. Zhou, M. S. Rzeszotarski, L. J. Singerman, and J. M. Chokreff, “The detection and quantification of retinopathy using digital angiograms,” *IEEE Trans. Med. Imag.*, vol. 13, no. 4, pp. 619–626, Dec. 1994.
- [5] C. Heneghan, J. Flynn, M. O’Keefe, and M. Cahill, “Characterization of changes in blood vessel width and tortuosity in retinopathy of prematurity using image analysis,” *Med. Image Anal.*, vol. 6, pp. 407–429, Oct. 2002.
- [6] A. M. Mendonça and A. Campilho, “Segmentation of retinal blood vessels by combining the detection of centerlines and morphological reconstruction,” *IEEE Trans. Med. Imag.*, vol. 25, no. 9, pp. 1200–1213, Sep. 2000.
- [7] S. Chaudhuri, S. Chatterjee, N. Katz, M. Nelson, and M. Goldbaum, “Detection of blood vessels in retinal images using two-dimensional matched filters,” *IEEE Trans. Med. Imag.*, vol. 8, no. 3, pp. 263–269, Sep. 1989.

- [8] M. G. Cinsdikici and D. Aydin, "Detection of blood vessels in ophthalmoscope images using mf/ant (matched filter/ant colony) algorithm," *Comput. Methods Programs Biomed.*, vol. 96, pp. 85–95, 2009.
- [9] X. Jiang and D. Mojon, "Adaptive local thresholding by verificationbased multi-threshold probing with application to vessel detection in retinal images," *IEEE Trans. Pattern Anal. Mach. Intell.*, vol. 25, no. 1, pp. 131–137, Jan. 2003.
- [10] T. McInerney and D. Terzopoulos, "T-snakes: Topology adaptive snakes," *Med. Imag. Anal.*, vol. 4, pp. 73–91, 2000.
- [11] L. Espona, M. J. Carreira, M. Ortega, and M. G. Penedo, "A snake for retinal vessel segmentation," *Pattern Recognition and Image Analysis, vol. 4478, Lecture Notes Comput. Sci.*, pp. 178–185, 2007.
- [12] M. E. Martinez-Perez, A. D. Hughes, S. A. Thom, A. A. Bharath, and K. H. Parker, "Segmentation of blood vessels from red-free and fluorescein retinal images," *Med. Imag. Anal.*, vol. 11, pp. 47–61, 2007.
- [13] B. S. Y. Lam and H. Yan, "A novel vessel segmentation algorithm for pathological retina images based on the divergence of vector fields," *IEEE Trans. Med. Imag.*, vol. 27, no. 2, pp. 237–246, Feb. 2008.
- [14] P. Bankhead, C. Scholfield, J. McGeown, and T. Curtis, "Fast retinal vessel detection and measurement using wavelets and edge location refinement." *PLoS One*, vol. 7, no. 3, pp. 1–12, 2012.
- [15] G. G. Gardner, D. Keating, T. H. Williamson, and A. T. Elliott, "Automatic detection of diabetic retinopathy using an artificial neural network: A screening tool," *Br. J. Ophthalmol.*, vol. 80, pp. 940–944, 1996.
- [16] C. Sinthanayothin, J. F. Boyce, H. L. Cook, and T. H. Williamson, "Automated localisation of the optic disc, fovea and retinal blood vessels from digital colour fundus images," *Br. J. Ophthalmol.*, vol. 83, pp. 902–910, 1999.
- [17] M. Niemeijer, J. Staal, B. v. Ginneken, M. Loog, M. D. Abramoff, J. Fitzpatrick, and E. M. Sonka, "Comparative study of retinal vessel segmentation methods

- on a new publicly available database,” *SPIE Med. Imag.*, vol. 5370, pp. 648–656, 2004.
- [18] J. Staal, M. D. Abrmoff, M. Niemeijer, M. A. Viergever, and B. v. Ginneken, “Ridge based vessel segmentation in color images of the retina,” *IEEE Trans. Med. Imag.*, vol. 23, no. 4, pp. 501–509, 2004.
- [19] J. V. B. Soares, J. J. G. Leandro, R. M. Cesar, H. F. J. Jr., and M. J. Cree, “Retinal vessel segmentation using the 2d gabor wavelet and supervised classification,” *IEEE Trans. Med. Imag.*, vol. 25, no. 9, pp. 1214–1222, 2006.
- [20] E. Ricci and R. Perfetti, “Retinal blood vessel segmentation using line operators and support vector classification,” *IEEE Trans. Med. Imag.*, vol. 26, no. 10, pp. 1357–1365, 2007.
- [21] D. Marn, A. Aquino, M. E. Gegndez-Arias, and J. M. Bravo, “A new supervised method for blood vessel segmentation in retinal images by using gray-level and moment invariants-based features,” *IEEE Trans. Med. Imag.*, vol. 30, no. 1, pp. 146–158, 2011.
- [22] T. Walter and J. C. Klein, “Segmentation of color fundus images of the human retina: Detection of the optic disc and the vascular tree using morphological techniques,” *Medical Data Analysis, ser. Lecture Notes in Computer Science*, J. Crespo, V. Maojo, and F. Martin, Eds. Berlin, Germany: Springer-Verlag,, pp. 282–287, 2001.
- [23] A. Hoover, V. Kouznetsova, and M. Goldbaum, “Locating blood vessels in retinal images by piecewise threshold probing of a matched filter response,” *IEEE Trans. Med. Imag.*, vol. 19, no. 3, pp. 203–210, Mar. 2000.
- [24] F. Zana and J. C. Klein, “Segmentation of vessel-like patterns using mathematical morphology and curvature evaluation,” *IEEE Trans. Image Process.*, vol. 10, no. 7, pp. 1010–1019, Jul. 2001.
- [25] A. Hoover and M. Goldbaum, “Locating the optic nerve in a retinal image using the fuzzy convergence of the blood vessels,” *IEEE Trans. Med. Imag.*, vol. 22, no. 8, pp. 951–958, 2003.



- [26] A. A. H. A. R. Youssif, A. Z. Ghalwash, and A. R. Ghoneim, "Optic disc detection from normalized digital fundus images by means of a vessels direction matched filter," *IEEE Trans. Med. Imag.*, vol. 27, no. 1, pp. 11–18, 2008.
- [27] D. Wu, M. Zhang, J.-C. Liu, , and W. Bauman, "On the adaptive detection of blood vessels in retinal images," *IEEE Trans. Biomed. Eng.*, vol. 53, no. 2,, pp. 341–343, 2006.
- [28] G. E. ien and P. Osnes, "Diabetic retinopathy: Automatic detection of early symptoms from retinal images," in *Proc. Norwegian Signal Processing Sym*, 1995.
- [29] R. C. Gonzalez, R. E. Woods, and S. L. Eddins, *Digital Image Processing Using Matlab*, 2nd ed. Kundli, Haryana: McGraw-Hill Education (India) Pvt Limited, 2012.
- [30] B. Zhang, X. Wu, Q. L. J. You, and F. Karray, "Detection of microaneurysms using multi-scale correlation coefficients," *Pattern Recognit.*, vol. 43, no. 1, pp. 2237–2248, 2010.
- [31] R. Jagoe, J. Arnold, C. Blauth, P. L. C. Smith, K. M. Taylor, and R. Wootton, "Measurement of capillary dropout in retinal angiograms by computerised image analysis," *Pattern Recognit.*, vol. 13, no. 1, pp. 143–151, 1992.